TaFT-D1 positively regulates grain weight by acting as a coactivator of TaFDL2 in wheat

Yinhui Zhang, Haixia Liu, Yaojia Wang, Xuemei Si, Yuxue Pan, Mengjiao Guo, Meijuan Wu, Yuanhao Li, Hongxia Liu (ID), Xueyong Zhang (ID), Jian Hou*, Tian Li* (ID) and Chenyang Hao* (ID)

State Key Laboratory of Crop Gene Resources and Breeding/National Key Facility for Crop Gene Resources and Genetic Improvement/Institute of Crop Sciences, Chinese Academy of Agricultural Sciences, Beijing, China

Summary

FLOWERING LOCUS T (*FT*), a multifunctional regulator in crops, modulates multiple key agronomic traits such as flowering time or heading date and plant height; however, its role in grain development regulation is unclear. Herein, through genome-wide association studies (GWAS), we identified *TaFT-D1*, which encodes a phosphatidylethanolamine-binding protein (PEBP), as a candidate gene for grain weight in wheat. A one-bp insertion/deletion (InDel) (G/-) in the third exon of *TaFT-D1*, resulting in different protein lengths, was significantly associated with grain weight. *TaFT-D1* knockout via the CRISPR-Cas9 system reduced grain size and weight, and *TaFT-D1* increased grain size by promoting cell proliferation and starch synthesis. Transcriptome analysis revealed a significant decrease in the expression of cell cycle- and starch synthesis-related genes, including *TaNAC019-3A*, *TaSWEET15-like-7B*, *TaCYCD4;1* and *TaCYCD3;2*, in the *taft-d1* knockout line. TaFT-D1 interacted with the bZIP transcription factor TaFDL2, and the *tafdl2* mutant presented relatively small grains, suggesting that TaFDL2 is a positive regulator of grain size. Moreover, TaFDL2 bound to the promoters of downstream cell cycle- and starch synthesis-related genes, activating their expression, whereas TaFT-D1 increased this activation via TaFDL2. Interaction assays demonstrated that TaFT-D1, Ta14-3-3A and TaFDL2 formed a regulatory complex. Furthermore, the *TaFT-D1(G)* allele was significantly correlated with greater thousand-grain weight and earlier heading. This favourable allele has undergone strong positive selection during wheat breeding in China. Our findings provide novel insights into how *TaFT-D1* regulates grain weight and highlight its potential application for yield improvement in wheat.

Introduction

As a well-known regulator of flowering, *FLOWERING LOCUS T* (*FT*) encodes a florigen protein that belongs to the phosphatidylethanolamine-binding protein (PEBP) family. FT transport within plants can occur over long distances, and FT plays a key role in the florigenic transition of plants during floral transformation (Liu *et al*., 2020a). As a conserved gene essential for flower induction, the overexpression of *FT* leads to early flowering in *Arabidopsis* (Kardailsky *et al*., 1999; Kobayashi *et al*., 1999). Similarly, in rice, the Hd3a protein promotes flowering by translocating from leaves to the apical meristem (Tamaki *et al*., 2007). However, as more *FT* homologues have been cloned and their functions have been identified across various species, it has become evident that these homologues can also inhibit flowering, modify plant architecture and increase yield in response to environmental changes (Jin *et al*., 2021). For example, the overexpression of soybean *GmFT4* in *Arabidopsis* delays flowering, indicating that this gene functions as a flowering suppressor and works in conjunction with *GmFT2a* and *GmFT5a* to regulate flowering in soybean (Zhai *et al*., 2022).

Additionally, *FT* influences plant morphology. In rapeseed, knocking out 1 to 4 of the five *BnFTL1* copies alters inflorescence structure and plant architecture, shortens the growth period and increases grain size (Wang *et al*., 2023). Furthermore, *FT* and its homologous genes significantly impact grain size and crop yield. In *Arabidopsis*, TERMINAL FLOWER1 (TFL1) delays endosperm development and increases grain size by affecting ABI5 stability (Zhang *et al*., 2020). In rice, the overexpression of *OsCEN2* (also known as *Rice TFL1/CEN* homologue, *RCN1*) reduces grain size, with 14-3-3 and FD2 acting as negative regulators (He *et al*., 2022). As a homologue of *FT*, *StSP6A* is crucial for flowering and tuber development in potato (Navarro *et al*., 2011). Furthermore, compared with wild-type (WT) wheat, *TaFT-D1*-knockout wheat presents a 2-3-day delay in heading date and a significantly greater spikelet number per spike (SN) (Chen *et al*., 2022). A recent study also confirmed that *TaFT-D1* regulates heading date, plant height and spikelet number per spike (Li *et al*., 2024a).

Increasing evidence indicates that FT acts as a small mobile protein that is transported between cells and tissues, contributing to its versatile functions in plants. Previous studies have shown

that *FT* is highly expressed in leaves and that its transport from companion cells to sieve elements is facilitated primarily by several regulatory pathways (Zicola *et al.*, 2019). One pathway for FT transport involves movement along the endoplasmic reticulum via plasmodesmata, a process mediated by the MCTP family protein FTIP1 (Shen *et al.*, 2024). An alternative pathway has been identified which involves the synergistic action of a membrane-localized SNARE protein, SYP21 and another protein of the MCTP family, QKY. This pathway is involved in the regulation of the directional transport of FT within the companion cell towards the cell membrane (Liu *et al.*, 2019). Additionally, the heavy metal-associated protein NaKR1, which is activated by CONSTANS (CO), plays a crucial role in the translocation of FT from the phloem to the apical meristem (Zhu *et al.*, 2016). Ultimately, FT binds to the FD protein, forming an activation complex that promotes the transcription of downstream target genes. In potato, the direct interaction of StSP6A with SWEET sugar transporter proteins modulates the source-sink balance (Abelenda *et al.*, 2019).

Wheat (*Triticum aestivum* L.) is a major staple crop globally, and its production is critical for food security. Grain weight is an important agronomic trait that significantly influences wheat yield, largely depending on grain size and filling. Grain weight is regulated by a complex and precise molecular network, and numerous genes related to grain weight have been cloned and characterized in wheat (Gao *et al.*, 2023). For example, TaGW2, an E3 ubiquitin ligase that is highly homologous to OsGW2, functions as a negative regulator of grain weight in wheat (Su *et al.*, 2011). TaDA1 has an additive effect with TaGW2 in regulating grain size and weight (Liu *et al.*, 2020b). *TaCKX2.1* and *TaCKX2.2*, which encode cytokinin oxidases, modulate both grain size and grain filling rates (Zhang *et al.*, 2012, 2024). Additionally, the sucrose synthase genes *TaSus1* and *TaSus2* are significantly associated with grain weight (Hou *et al.*, 2014; Jiang *et al.*, 2011). TaTPP-7A promotes starch synthesis and grain filling through the T6P-SnRK1 pathway and sugar-ABA interactions (Liu *et al.*, 2023). Furthermore, *TaNAC019* knockout results in reduced starch and protein contents, leading to decreased grain weight (Gao *et al.*, 2021). The genes involved in the regulation of grain weight can be categorized into different pathways, including transcriptional regulation, posttranslational modifications, starch synthesis and signalling pathways such as the G protein and plant hormone pathways (Gao *et al.*, 2023). However, most wheat grain weight genes have been primarily cloned through comparative genomics approaches, highlighting the need to explore and apply new genes while also deepening our understanding of the genetic mechanisms underlying grain weight regulation.

In this study, *TaFT-D1* was identified through a genome-wide association studies (GWAS) as a candidate gene for determining wheat grain weight. A single base pair variation (G/-) in the third exon of *TaFT-D1*, which results in the production of full-length or truncated proteins, was significantly associated with grain weight. Knocking out *TaFT-D1* via the CRISPR-Cas9 gene editing method led to reduced grain size and weight. Further analysis revealed that TaFT-D1 interacted with the bZIP transcription factor TaFDL2, promoting the activation of target genes involved in the cell cycle and starch synthesis. Additionally, the *TaFT-D1(G)* allele was significantly associated with increased thousand-grain weight and an earlier heading date and has undergone strong positive selection during wheat breeding in China. Overall, our findings enhance our understanding of the function of *FT* and

provide new insights into the regulation of grain weight by *TaFT-D1*.

Results

TaFT-D1 is a candidate gene for determining grain weight

A natural population composed of 476 accessions was genotyped via a Wheat660K SNP array (Affymetrix Axiom Wheat660), and 350 497 high-quality SNPs previously obtained were used in this study. These SNPs were integrated with phenotypic data related to thousand-grain weight (TGW), plant height (PH) and heading date (HD), which were collected across multiple environments, to perform genome-wide association studies (GWAS) and multiple significant signals ($-\log_{10}(P) \geq 4$) of TGW, PH and HD were detected simultaneously on the short arm of chromosome 7D (Figures 1a and S1a). The peak SNPs were located primarily between 68.721 Mb and 70.721 Mb (Figures 1b and S1b). In this interval, 13 high-confidence genes were identified (Table S1). The expression levels of these genes across various tissues were predicted using the Wheat Expression Browser (http://wheat-expression.com) (Figures 1c and S1c), which revealed that only four genes presented high expression levels. Among these four genes, sequence variations were detected in the coding regions of *TraesCS7D02G111500* and *TraesCS7D02G111600* on the basis of resequencing data from 145 landmark cultivars (http://wheat.cau.edu.cn/WheatUnion) (Hao *et al.*, 2020), and a synonymous mutation was identified in *TraesCS7D02G111500* (Figure S2a). However, the variation in *TraesCS7D02G111600* involved a single nucleotide (G/-) insertion and deletion (InDel) in its third exon (Figures 1d and S1d). *TraesCS7D02G111600* was annotated as *FLOWERING LOCUS T* (*FT*) and was thus designated *TaFT-D1*. Phenotypic analysis of 145 landmark cultivars between the two *TaFT-D1* alleles *TaFT-D1(-)* and *TaFT-D1(G)* revealed that the mean TGW of *TaFT-D1(-)* accessions was significantly lower than that of *TaFT-D1(G)* accessions, whereas the mean PH and HD of *TaFT-D1(-)* accessions were significantly greater than those of *TaFT-D1(G)* accessions (Figures 1e and S1e). Meanwhile, phenotypic analyses of *TraesCS7D02G111500* alleles from 145 landmark cultivars showed that it was just associated with PH (Figure S2b). Collectively, these results suggest that *TaFT-D1* may be a candidate gene that controls the traits TGW, PH and HD.

TaFT-D1 positively regulates wheat grain size and weight

Subsequent analyses revealed that *TaFT-A1*, *TaFT-B1* and *TaFT-D1* all consisted of three exons (Figure S3a). The 1-bp deletion in *TaFT-D1(-)* resulted in a frameshift mutation (Figure S3b). RT-qPCR analysis revealed that *TaFT-D1* was predominantly expressed in flag leaves (Figure S3c). Subcellular localization assays revealed that TaFT-D1(G)-GFP was distributed throughout the cytoplasm and nucleus, whereas TaFT-D1(-)-GFP was distributed only in the cytoplasm (Figure S3d).

To determine the biological function of *TaFT-D1* in wheat grain, *TaFT* homoeologs were edited via CRISPR-Cas9 technology in the Kenong 199 (KN199) wheat cultivar (Figure S4a). Five *TaFT* knockout lines were identified through sequencing: two lines with mutations in *TaFT-D1* (AABBdd), one line with mutations in *TaFT-B1* (AAbbDD), one line with mutations in both *TaFT-A1* and *TaFT-B1* (aabbDD) and one line with mutations in *TaFT-A1*, *TaFT-B1* and *TaFT-D1* (aabbdd); these lines were designated *taft-1*, *taft-2*, *taft-3*, *taft-4* and *taft-5*, respectively (Figure S4b). Protein
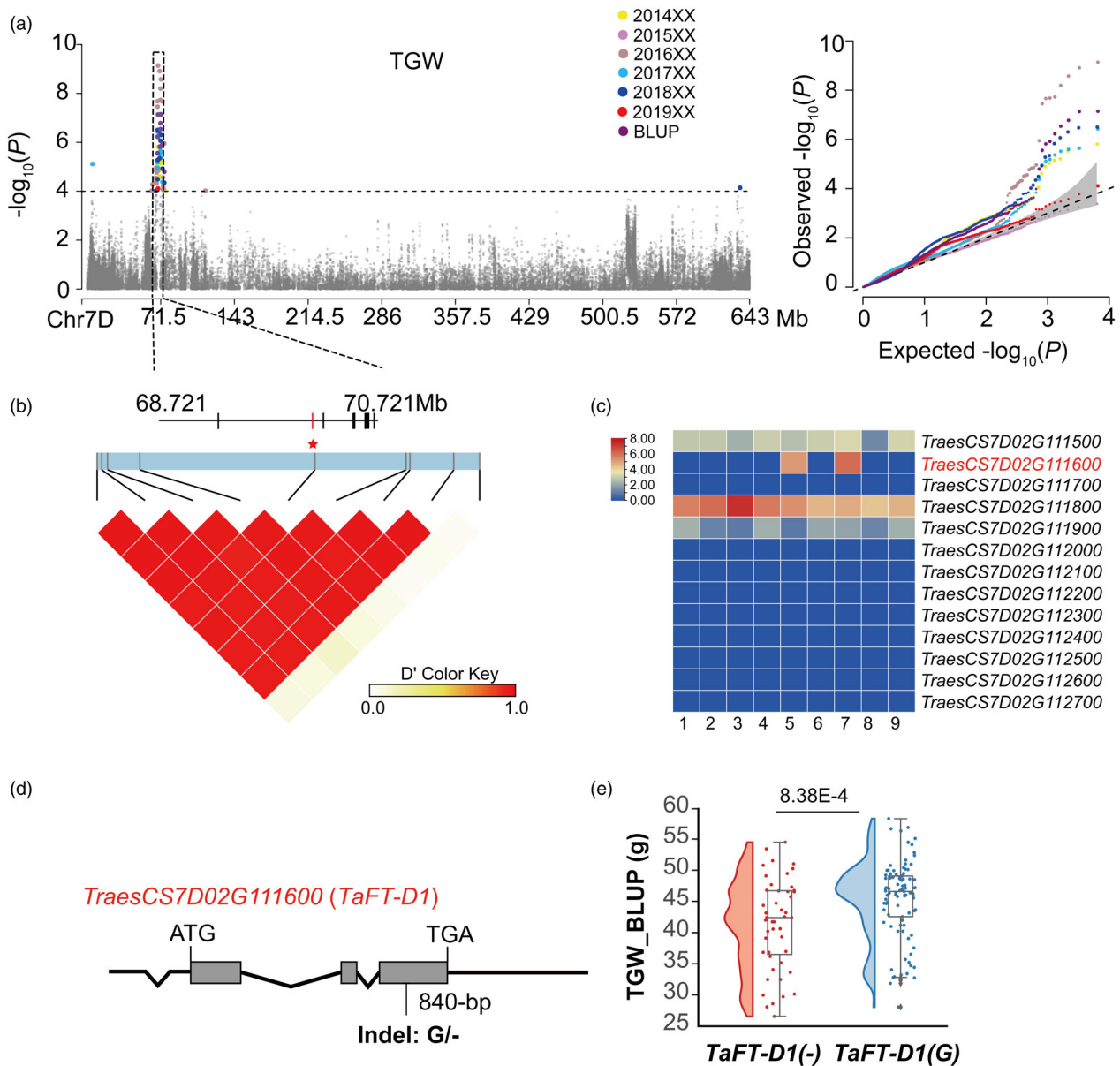
Figure 1 *FT-D1* was identified as a candidate gene controlling thousand-grain weight (TGW) on chromosome 7D through GWAS. (a) Manhattan and QQ plots showing significant associations with TGW on chromosome 7D for multiple environments. The black dashed line represents the threshold value. (b) Linkage disequilibrium diagram for peak SNPs. The black line at the top indicates the locations of candidate genes within this region, and the red star highlights the specific position of the candidate gene *TaFT-D1*. (c) Predicted expression profiles of 13 candidate genes in this region at different developmental phases and tissues according to an online public database (https://www.wheat-expression.com/). 1, roots, seedling ($n = 8$); 2, leaves/shoots, seedling ($n = 174$); 3, leaves/shoots, vegetative ($n = 156$); 4, roots, vegetative ($n = 73$); 5, leaves/shoots, reproductive ($n = 151$); 6, roots, reproductive ($n = 8$); 7, spike, reproductive ($n = 278$); 8, grain, reproductive ($n = 166$); and 9, spike, vegetative ($n = 2$). (d) Gene structure and key mutation sites of the candidate gene *TaFT-D1*. (e) Cloud and rain plot showing that *FT-D1(G)* has a significantly higher TGW BLUP value than does *FT-D1(−)*. A natural population (NP) of 145 landmark cultivars were classified on the basis of a single nucleotide (G) insertion and deletion (InDel) in *TaFT-D1*. The scatter points represent these cultivars.

sequence analysis reveals that both natural variations and gene editing-induced mutations result in frameshift mutations in the FT-D1 protein, altering its sequence compared to the WT protein and leading to a loss of function of FT-D1 (Figure S4c).

Phenotypic assessments of these *taft* lines in the field revealed that the HD of *taft-1, -2, -3, -4* and *-5* was progressively delayed as more *TaFT* homoeologs were knocked out (Figure 2a). Compared with the WT, the *taft-1* and *taft-2* lines presented

HD approximately 2 days later, whereas the HD of the *taft-5* line was delayed by 15 days (Figure 2b). The TGW of *taft-1* and *taft-2* was lower than that of the WT, decreasing by 7.7% and 10.3%, respectively (Figure 2c,d). Notably, the differences in TGW between the WT and *taft-1/-2* lines were attributed primarily to grain width (GW) rather than grain length (GL). Additionally, the effective tiller number (ETN), spikelet number per spike (SN) and grain number per spike (GNS) differed significantly between the
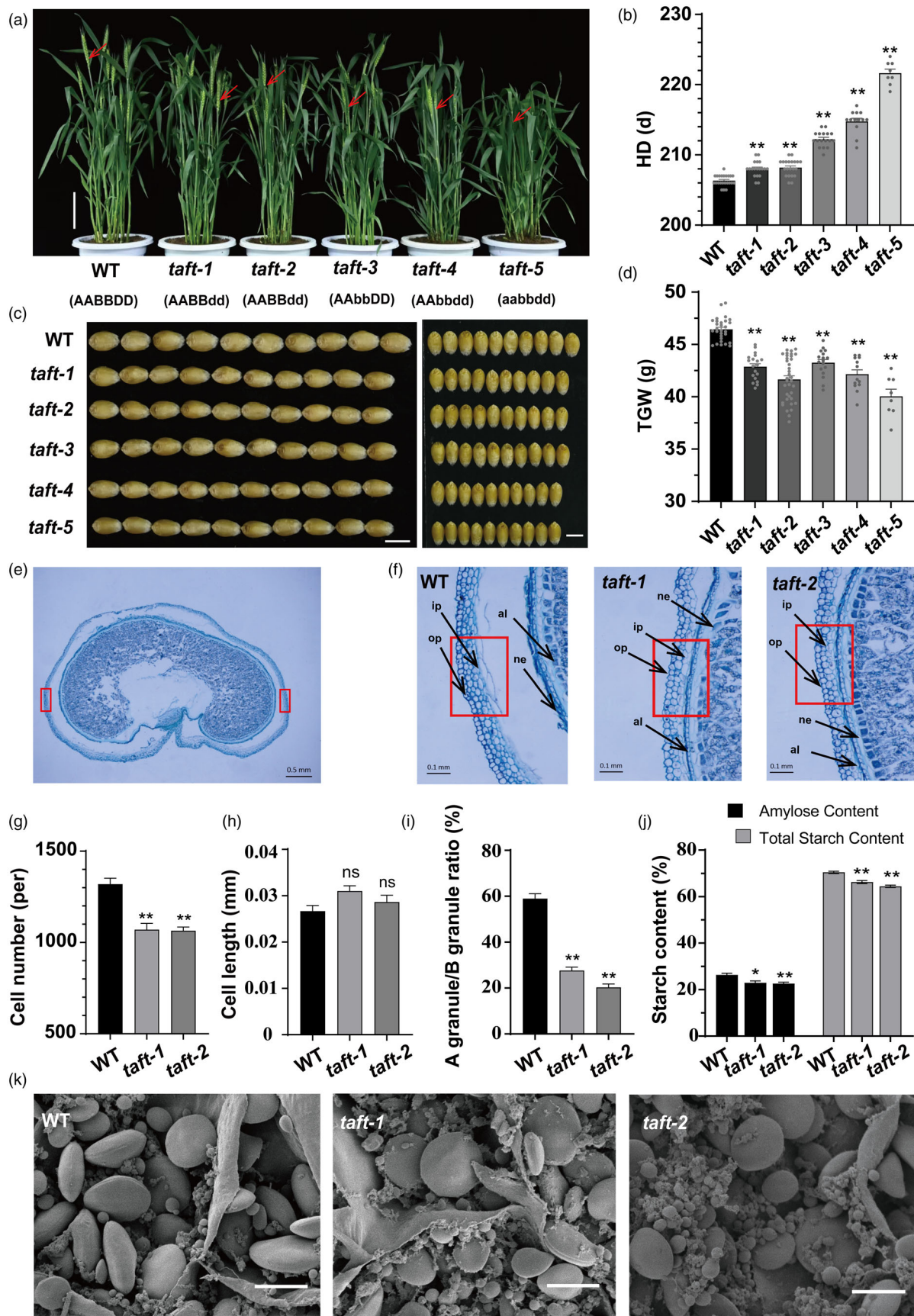
Figure 2 Knockout of *TaFT-D1* leads to later heading dates and lower thousand-grain weights. (a, b) Comparison of the phenotypes and heading dates (HDs) between the WT and *taft* lines grown in the field under natural conditions. Red arrows indicate spikes. Bar = 10 cm. (c, d) Comparison of the grain size between the WT and *taft* lines. Bars = 5 mm. (n_{WT} = 29, n_{taft-1} = 19, n_{taft-2} = 36, n_{taft-3} = 17, n_{taft-4} = 13, n_{taft-5} = 8) in (a)–(d). (e) A representative section of the middle portion of a developing grain of KN199 (WT) wheat at 15 days post-anthesis (DPA). Bar = 0.5 mm. (f) Comparison of the outer pericarp cells in the *taft-1*, *taft-2* and WT lines. Each image was captured from the boxed areas indicated in (e). op: outer pericarp; ip: inner pericarp; ne: nucellar epidermis; and al: aleurone layer. Bars = 0.1 mm. (g, h) Comparison of cell number and cell length in the outer pericarp tissues of the *taft-1*, *taft-2* and WT lines. (*n* = 3) in (e)–(h). (i) A-granule/B-granule ratios in the grains of the *taft-1*, *taft-2* and WT lines. (j) Amylose content and total starch content in the grains of the *taft-1*, *taft-2* and WT lines. (k) Scanning electron microscopy of starch granules in the 20 DPA endosperm of the *taft-1*, *taft-2* and WT lines. Bars = 20 μm. (*n* = 3) in (i)–(k). All values are presented as means ± SD. * and ** indicate significant differences from the WT at *P* < 0.05 and *P* < 0.01 (ANOVA), respectively.

WT and mutant lines (Figure S4d). Under greenhouse conditions, the HD of *taft-1* and *taft-2* was delayed by 2–3 days and the TGW was lower by 10.4% and 13.5%, respectively, compared with those observed in the WT line (Figure S5a–c). Taken together, these results demonstrate that *TaFT-D1* positively regulates wheat grain size and weight.

TaFT-D1 promotes cell proliferation and starch synthesis in wheat grain

The changes in the grain size and weight of the mutant lines may be attributed to variations in cell proliferation and the grain-filling process. The grain coat cells of *taft-1*, *taft-2* and WT lines were subsequently observed at 15 days post-anthesis (DPA) (Figure 2e). Compared with those in the WT, the numbers of grain coat cells and cell layers in *taft-1* and *taft-2* were lower, resulting in a narrower grain coat cell layer (Figure 2f). Statistical analysis revealed that the cell numbers in the grain coats of *taft-1* and *taft-2* were approximately 18.9% and 19.4% lower, respectively, than those in the WT (Figure 2g). However, the cell length did not change significantly (Figure 2h).

Next, the starch granules of developing grains at 20 DPA were compared among the WT, *taft-1* and *taft-2* lines. Scanning electron microscopy revealed that the arrangement of starch granules in *taft-1* and *taft-2* was looser than that in the WT and that the proportions of A-type and B-type starch granules changed significantly (Figure 2k). Specifically, the number of A-type starch granules in the *taft-1* and *taft-2* lines decreased, whereas the number of B-type starch granules increased (Figure 2i). Additionally, the amylose contents in *taft-1* and *taft-2* decreased by 12.9% and 14.2%, respectively, whereas the total starch content decreased by 5.9% and 8.5%, respectively (Figure 2j). These results confirm that *TaFT-D1* positively regulates grain size and weight by promoting cell proliferation and starch synthesis.

TaFT-D1 protein enters wheat grain as a mobile protein

To investigate how *TaFT-D1* regulates wheat grain size and weight, transcriptome sequencing was conducted using grains from both the WT and *taft-d1* lines at 15 DPA. This analysis revealed 1964 downregulated and 1396 upregulated differentially expressed genes (DEGs) in the *taft-d1* line compared with the WT line (Figure 3a; Table S2). These DEGs were enriched in multiple biological processes, including the cell cycle, cell wall modification and starch biosynthetic (Figure S6a). Many genes known to influence wheat grain weight and size were significantly downregulated in the *taft-d1* line, a finding that is consistent with its relatively small-grain phenotype. Four genes were involved mainly in starch synthesis and the cell cycle: *TaNAC019-3A*, *TaSWEET15-like-7B*, *TaCYCD4;1* and *TaCYCD3;2*

(Figure 3b). These four downstream genes were further examined via RT-qPCR in developing grains of the WT, *taft-1* and *taft-2* lines. The results indicated that, compared with those in the WT, the expression levels of these four genes were significantly lower in the grains of the *taft-d1* lines (Figure 3c). Additionally, several genes encoding positive regulators of grain weight and size, such as *TaSus1-like*, *TaABI5-like*, *TaCKX1*, *TaSCPL18*, *TaD11*, *TaCKX2.2* and *TaMYB70*, also presented reduced expression in the *taft-1* and *taft-2* lines (Figure S6b).

However, the expression of *TaFT-D1* could not be detected in grains by either RNA-seq or RT-qPCR (Figures 3d and S3c). Given that FT could function as a mobile protein transported to other organs, it was hypothesized that TaFT-D1, a small-molecule protein, moves from leaves into grains to exert its function. To test this hypothesis, proteomic analysis of grains at 15 DPA for both the WT and *taft-d1* lines was subsequently conducted. The results indicated that the TaFT-D1 protein along with other proteins were specifically expressed in grains. The protein level of TaFT-D1 in the *taft-d1* line was lower than that in the WT line (Figure 3e; Table S3). Thus, the TaFT-D1 protein likely enters wheat grains as a mobile protein and influences the expression of genes involved in the cell cycle and starch synthesis.

TaFT-D1 interacts with TaFDL2, a positive regulator of grain size and weight

Four *TaFDL* genes that are expressed in grains were analysed (Figure S7) to determine whether FT can interact with FD-like (FDL) proteins and coregulate grain and tuber size in wheat. Among these genes, *TaFDL2* and *TaFDL6* were predominantly expressed in developing and mature grains. The interaction between TaFT-D1 and TaFDL2 was confirmed via a yeast two-hybrid (Y2H) assay (Figure 4a). Next, firefly luciferase complementation imaging (LCI) and bimolecular fluorescence complementation (BiFC) assays were performed in *Nicotiana benthamiana*. Significant LUC activity was observed in cells coexpressing TaFT-D1-cLUC and TaFDL2-nLUC (Figure 4b). Additionally, a yellow fluorescent protein (YFP) signal was detected in the nucleus of cells coexpressing cYFP-TaFDL2 and nYFP-TaFT-D1 (Figure 4c), but no signals were detected in the negative controls, indicating a physical interaction between TaFT-D1 and TaFDL2.

When a TaFDL2-GFP fusion protein was transiently expressed, the green fluorescence signal was localized exclusively in the nucleus, indicating that TaFDL2 is a nucleus-localized protein (Figure S8a). To analyse the transcriptional activity of TaFDL2, TaFDL2 was cloned and inserted into a 35S-GAL4DB-NOS vector to serve as an effector. The herpes simplex virus protein VP16 and the 35S-GAL4DB empty vector were used as positive and negative controls, respectively. The transient expression of TaFDL2 in *N. benthamiana* resulted in significantly greater

(a)

(b)

(c) TaNAC019-3A TaSWEET15-like-7B TaCYCD3;2 TaCYCD4;1

(d)

(e)
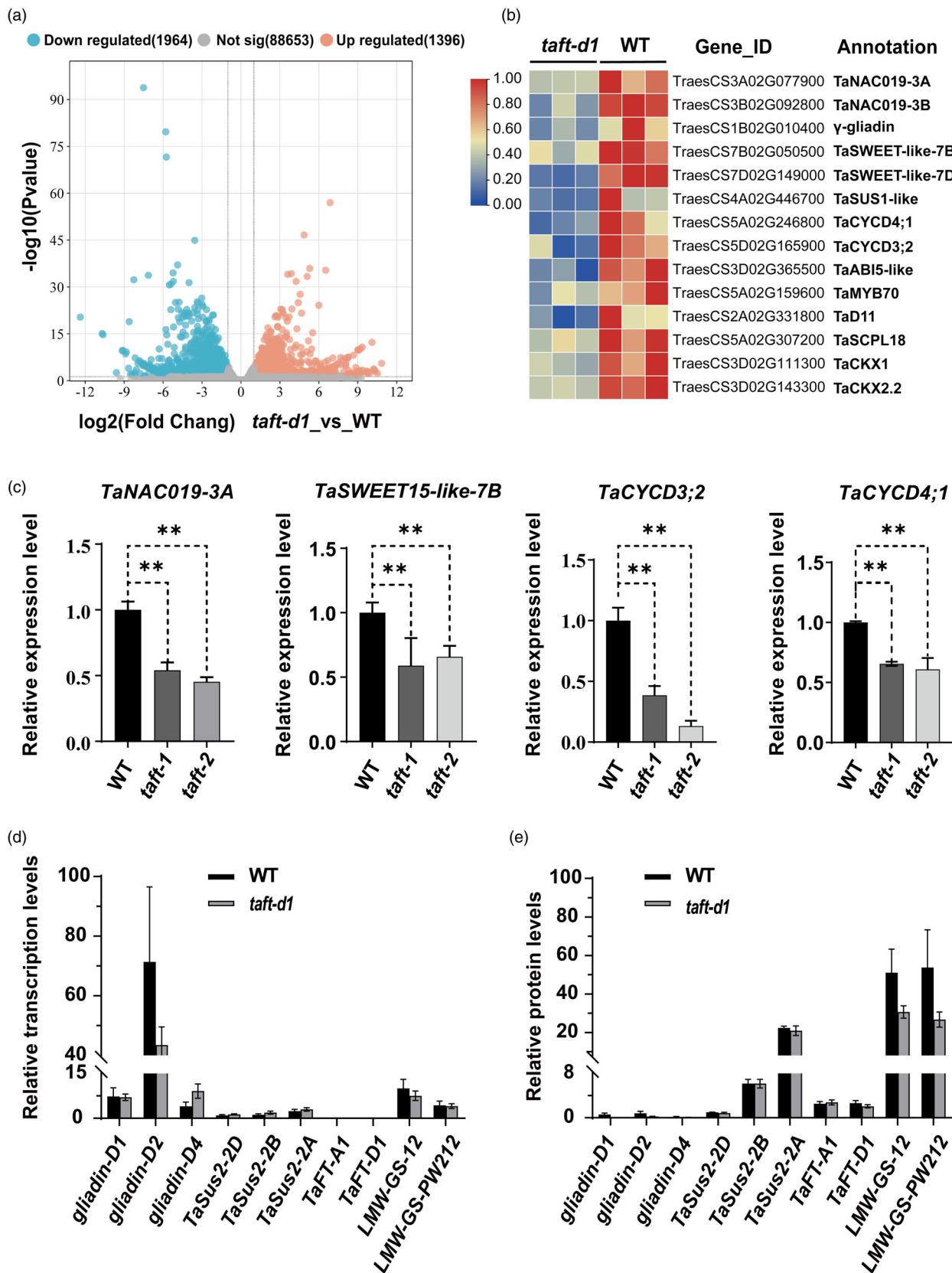
Figure 3 Transcriptome and RT–qPCR analyses of differentially expressed genes between the WT and *taft-d1* lines, along with the proteome identification of FT proteins in grains. (a) Volcano plot illustrating the number of differentially expressed genes (DEGs) among grains collected at 15 days post-anthesis (DPA) from the WT and *taft-d1* lines, as identified via transcriptome analysis. Red and blue points indicate upregulated genes and downregulated genes, respectively. (b) Heatmap showing that the expression of genes involved in the regulation of the cell cycle and starch synthesis was significantly downregulated in the *taft-d1* line. (c) RT–qPCR analysis of four representative downregulated genes in the grains of the WT and *taft-d1* lines at 15 DPA (*n* = 3). (d) Transcriptome analysis of the relative expression of *TaFT1* and other genes in the grains of the WT and *taft-d1* lines at 15 DPA. (e) Proteomic analysis confirming the presence of TaFT1 proteins in the grains of the WT and *taft-d1* lines at 15 DPA. All values are presented as means ± SD. * and ** indicate significant differences from the WT at *P* < 0.05 and *P* < 0.01 (ANOVA), respectively.

transcriptional activity than did the transient expression of the empty vector (Figure S8b). Therefore, TaFDL2 acts as a transcriptional activator in wheat grain.

To verify the regulatory role of *TaFDL2* in wheat grain size, a *tafdl2* mutant was obtained from the hexaploid wheat variety KN9204 mutant library. A G-to-A mutation at 534 bp of *TaFDL2-1B* was identified in the *tafdl2-1b* line, leading to premature termination of translation (Figure S8c). Compared with that of the KN9204 control, the GW of *tafdl2-1b* was significantly lower, whereas the GL was not significantly different (Figure 4d). More importantly, the TGW of *tafdl2-1b* decreased by 7.3% compared with that of the WT, with no significant difference in HD (Figure 4e). These results indicate that *TaFDL2-1B* positively regulates TGW and GW in wheat.

TaFDL2 binds to the promoters of downstream genes regulated by TaFT-D1

Since the bZIP transcription factor FDL can bind to G-box/G-box-like motifs, we examined whether TaFDL2 regulates the four DEGs associated with *taft-1*. Promoter analysis revealed that several G-box and G-box-like motifs were present within the promoters of *TaNAC019-3A*, *TaSWEET15-like-7B*, *TaCYCD4;1* and *TaCYCD3;2* (Figure 5a). A yeast one-hybrid assay (Y1H) was subsequently conducted by cloning the promoter regions of each downstream gene into the pLacZi vector and transforming the constructs into the yeast strain EGY48 along with TaFDL2-pB42AD. After 3 days of growth, the cotransformed yeast successfully survived and turned blue on SD/-Trp/-Ura/X-gal medium (Figure 5b). The results were confirmed by electrophoretic mobility shift assay (EMSA), the results of which demonstrated that the His-TaFDL2 recombinant protein (but not the His-tag alone) could bind to the promoters of the downstream genes; however, it could not bind to promoters containing mutated binding elements (Figure 5c). In summary, both the Y1H assays and EMSA demonstrated that TaFDL2 can bind to the promoters of *TaNAC019-3A*, *TaSWEET15-like-7B*, *TaCYCD4;1* and *TaCYCD3;2*.

### TaFT-D1 acts as a coactivator of TaFDL2 in the regulation of downstream genes

Given that the 14-3-3 protein can interact with FT and FDL in rice and potato, further investigation was performed to determine whether the Ta14-3-3 protein interacts with TaFT-D1 and TaFDL2 in wheat. Among the *Ta14-3-3A*, *B* and *D* isoforms, *Ta14-3-3A* was expressed at higher levels than the other two in all the examined tissues (Figure S9). The Y2H assay results indicated that Ta14-3-3A interacted with both TaFT-D1 and TaFDL2 (Figure 6a). Both LCI and BiFC assays revealed significant LUC activity in cells coexpressing TaFT-D1-cLUC and Ta14-3-3A-nLUC, as well as in cells coexpressing Ta14-3-3A-cLUC and TaFDL2-nLUC (Figure 6b). Additionally, YFP signals were observed in the cell membrane and nucleus of cells coexpressing cYFP-Ta14-3-3A and nYFP-TaFT-D1.

Signals were also detected in the nuclei of cells coexpressing cYFP-Ta14-3-3A and nYFP-TaDL2 (Figure 6c). The interaction between TaFT-D1(-) and Ta14-3-3A was also evaluated in cotransformed yeast cells, but no interaction between them was observed (Figure 6d). This lack of interaction suggests that premature termination caused by the frameshift mutation may disrupt complex formation. These results indicate that the Ta14-3-3A protein interacts with both TaFT-D1 and TaFDL2 to form a trimer complex.

To clarify the effects of TaFT-D1, Ta14-3-3A and the TaFDL2 complex on the expression of downstream genes, a series of transient expression assays were conducted in *N. benthamiana*. Effector vectors for TaFT-D1, TaFDL2 and Ta14-3-3A, along with LUC reporter vectors driven by 2-kb promoter regions of downstream genes, were constructed (Figure 6e). Compared with the control, TaFDL2 alone activated the expression of downstream genes, resulting in a 3-4-fold increase in LUC reporter activity, confirming that TaFDL2 is a transcriptional activator. In contrast, the addition of Ta14-3-3A inhibited the expression of downstream genes. Notably, when TaFT-D1 was included, the inhibitory effect of Ta14-3-3A was diminished. The highest expression of downstream genes was observed when only TaFT-D1 and TaFDL2 were present (Figure 6f). Consistent with the fact that TaFT-D1(-) does not interact with TaFDL2 and co-expression of TaFT-D1(-) has no effect on the transactivation of downstream genes by TaFDL2 (Figure S10). These results suggest that TaFT-D1 functions as a coactivator of TaFDL2 in the regulation of downstream genes.

TaFT1 homoeologs may exhibit functional divergence

To identify *TaFT-D1(G)* and *TaFT-D1(-)* alleles, a Kompetitive Allele Specific PCR (KASP) marker was developed on the basis of a single-nucleotide InDel (G/-) located 840-bp downstream of the ATG start codon. This marker accurately distinguished the two alleles of *TaFT-D1* (Figure S11a). After genotyping with this marker, the mean TGW and GW significantly differed between the two alleles of *TaFT-D1* in 157 Chinese landraces and 348 modern Chinese cultivars (Table S4). Specifically, the TGW of *TaFT-D1(G)* increased by 4.1–5.0 g compared with that of *TaFT-D1(-)*, whereas the GW of *TaFT-D1(G)* increased by 2.8%–4.6% (Figure 7a). The other traits, such as SN, GNS and PH, of *TaFT-D1(G)* were lower than those of *TaFT-D1(-)*, and the HD of *TaFT-D1(G)* occurred 2–3 days earlier (Figure S11b). Furthermore, the proportion of *TaFT-D1(G)* significantly increased from landraces to modern cultivars, indicating that *TaFT-D1(G)* underwent strong positive selection during the wheat breeding process in China (Figure 7b). From the 1940s to the 2000s, the frequency of *TaFT-D1(G)* increased from 50% to 97.6%, whereas the frequency of *TaFT-D1(-)* gradually decreased from 50% to 2.4% (Figure 7c). By contrast, most common wheat accessions from foreign countries carried the *TaFT-D1(-)* allele (Figure 7d; Table S5).

8 *Yinhui Zhang* et al.
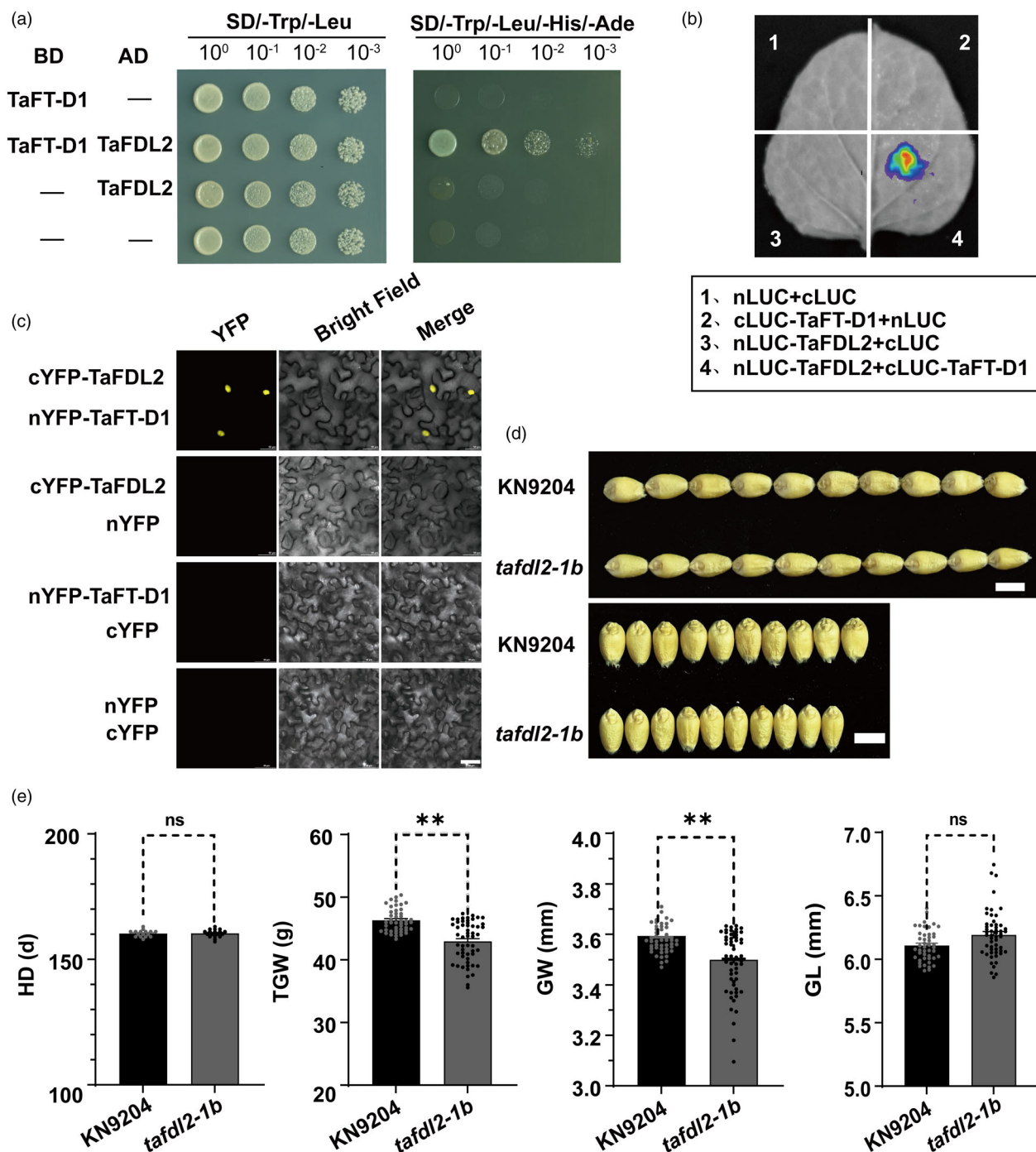
Figure 4 TaFT-D1 interacts with TaFDL2, a positive regulator of grain size and weight. (a) Confirmation of the interaction between TaFT-D1 and TaFDL2 via yeast two-hybrid assays. SD/-Trp/-Leu, synthetic dextrose medium lacking Trp and Leu; SD/-Trp/-Leu/-His/-Ade, synthetic dextrose medium lacking Trp, Leu, His and Ade. The dilution series are represented as 10^0–10^{-3}. (b) Luciferase complementation imaging (LCI) assays were used to assess the physical interaction between TaFT-D1 and TaFDL2 in the epidermal cells of *N. benthamiana* leaves. nLUC, N-terminal portion of luciferase (LUC); cLUC, C-terminal portion of LUC. The LUC signals were collected 48–72 h after infiltration. (c) Bimolecular fluorescence complementation (BiFC) assays were used to assess the *in vivo* interaction between TaFT-D1 and TaFDL2 in the nuclei of *N. benthamiana* epidermal cells. nYFP, N-terminal portion of yellow fluorescence protein (YFP); cYFP, C-terminal portion of YFP. Bars = 20 μm. (d) Photographs of the grain lengths and widths of WT (KN9204) and the mutant *tafdl2-1b*. Bars = 0.5 cm. (e) Comparisons of heading date (HD), thousand-grain weight (TGW), grain length (GL) and grain width (GW) between the WT and *tafdl2-1b* mutant. ($n_{WT} = 46$, $n_{tafdl2-1b} = 54$) in (d) and (e). ** indicates a significant difference from the WT at $P < 0.01$ (Student's t-test), and 'ns' indicates no significant difference ($P > 0.05$).

With respect to *TaFT-D1* homologous genes, *TaFT-A1* presented two alleles, that is, *TaFT-A1(T)* and *TaFT-A1(G)* (Figure S12a,c), as did *TaFT-B1*, that is, *TaFT-B1(G)* and *TaFT-B1*

(C) (Figure S13a,c). Two derived cleaved amplified polymorphic sequence (dCAPS) markers were developed for *TaFT-A1* and *TaFT-B1*. Unlike *TaFT-D1*, which was significantly associated with
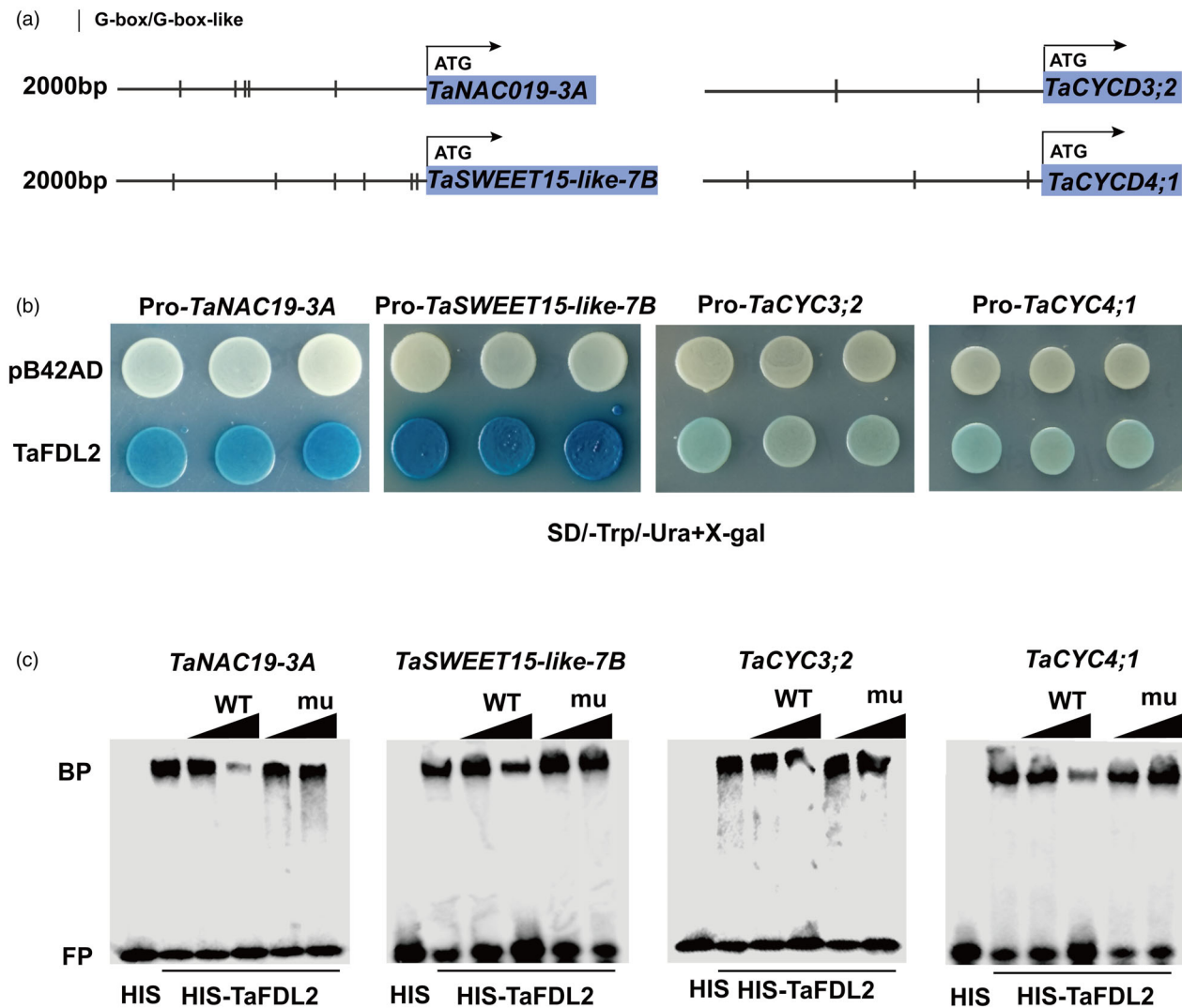
Figure 5 TaFDL2 binds to the promoters of downstream candidate genes. (a) Identification of TaFDL2 binding sites (G-box and G-box-like binding sites) in the promoters of distinct downstream genes, including *TaNAC19-3A, TaSWEET15-like-7B, TaCYC3;2* and *TaCYC4;1*. (b) Interaction of TaFDL2 with specific cis-elements, as assessed via yeast one-hybrid assays. The pB42AD empty vector and pLacZi-TaFDL2 were cotransformed as controls. (c) Electrophoretic mobility shift assay (EMSA) was used to assess whether TaFDL2 binds to the promoter sequences of *TaNAC19-3A, TaSWEET15-like-7B, TaCYC3;2* and *TaCYC4;1 in vitro*. Competition assays were performed using unlabeled 10× and 100× wild-type (WT) and motif-mutated (mu) probes. 'BP' is bound probe; 'FB' is free probe.

TGW and GW, *TaFT-A1* was significantly correlated with PH and HD (Figure S12b), with phenotypic effect values of −20.64 cm and −4.41 days (Table S6), and phenotypic variance explained 8.11% and 10.74%, respectively (Table S7). The corresponding values were relatively low in *TaFT-B1*, except for GNS (Figure S13b; Tables S6 and S7). Taken together, these results suggest that *TaFT-A1*, *TaFT-B1* and *TaFT-D1* may exhibit functional divergence for important agronomic traits in wheat.
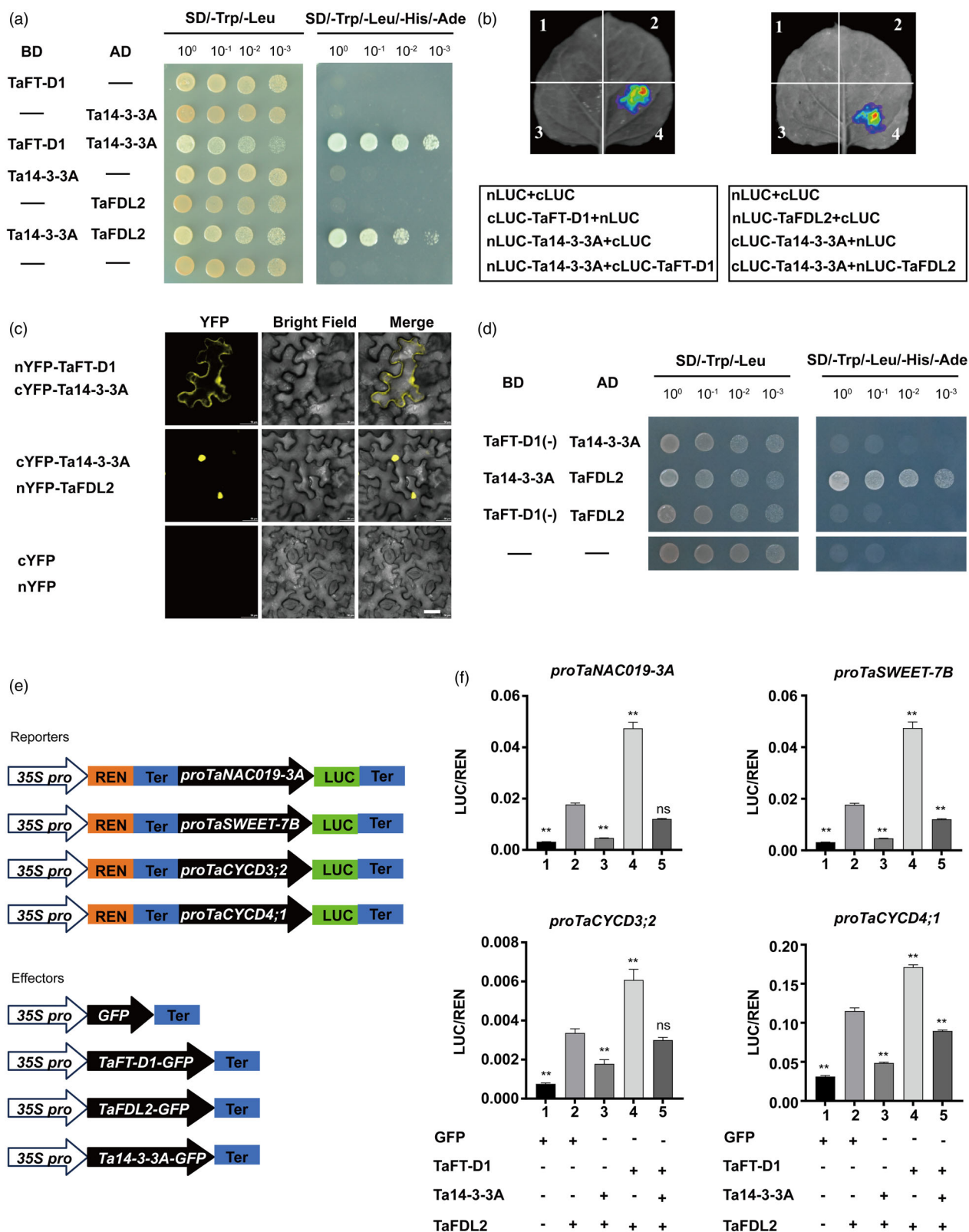
Discussion

The TaFT-D1-Ta14-3-3A-TaFDL2 module regulates the TGW of wheat

The grain weight of wheat is regulated by multiple genes and their associated modules. Identifying key genes that regulate grain size and weight in wheat and elucidating their molecular

mechanisms hold significant value for improving crop yields. An increasing number of regulatory modules influencing grain weight have been reported. For example, TaIAA21 participates in wheat grain development through the ARF25-ERFs module (Jia et al., 2021). TaSnRK1 and TabHLH489 integrate brassinosteroid and sugar signalling to regulate wheat grain size (Lyu et al., 2024). In this study, *TaFT-D1* positively regulated both grain weight and grain size (Figure 2). More interestingly, proteomic analysis indicated that TaFT-D1 may function as a mobile protein transported from the leaves (Figure 3). The transport of FT protein from companion cells to sieve elements occurs mainly through several regulatory pathways. Specifically, the transport of FT from phloem companion cells to sieve tubes occurs via two main parallel transport systems: FTIP1-mediated ER transport (Shen et al., 2024) and endosomal vesicle transport mediated by QKY and SYP121 (Liu et al., 2019). The subsequent

long-distance transport of FT in the vascular system is influenced primarily by NaKR1 (Zhu et al., 2016). In addition, the interaction between StSP6A (a homologous gene of *FT*) and the sucrose transporter StSWEET11 in potato prevents the leakage of sucrose, likely promoting sucrose transport into plastids (Abelenda et al., 2019). In wheat, TaFT-D1 can interact with the transport

© 2025 The Author(s). *Plant Biotechnology Journal* published by Society for Experimental Biology and The Association of Applied Biologists and John Wiley & Sons Ltd., 1–17

Figure 6 TaFT-D1 promotes the activation of downstream target genes via TaFDL2. (a) Analysis of the interaction between TaFT-D1, Ta14-3-3A and TaFDL2 via yeast two-hybrid (Y2H) assays. SD/-Trp/-Leu, synthetic dextrose medium lacking Trp and Leu; SD/-Trp/-Leu/-His/-Ade, synthetic dextrose medium lacking Trp, Leu, His and Ade. The dilution series are represented as 10^0–10^{-3}. (b) Luciferase complementation imaging (LCI) assays were used to analyse the physical interaction between TaFT-D1, Ta14-3-3A and TaFDL2 in the epidermal cells of *N. benthamiana* leaves. nLUC, N-terminal portion of luciferase (LUC); cLUC, C-terminal portion of LUC. (c) Bimolecular fluorescence complementation (BiFC) assays were performed to assess the *in vivo* interaction between TaFT-D1, Ta14-3-3A and TaFDL2 in the nuclei of tobacco epidermal cells. nYFP, N-terminal portion of yellow fluorescence protein (YFP); cYFP, C-terminal portion of YFP. Bars = 50 μm. (d) Evaluation of the interaction between TaFT-D1(-), Ta14-3-3A and TaFDL2 via Y2H assays. (e) Schematic diagrams of the reporters and effectors used in the transient expression assay. 35S pro, CaMV 35S promoter; LUC, firefly luciferase; REN, Renilla luciferase; ter, terminator. (f) Transient expression assays in *N. benthamiana* leaves were used to assess whether TaFDL2 activates the transcription of *TaNAC19-3A*, *TaSWEET15-like-7B*, *TaCYC3;2* and *TaCYC4;1*. Ta14-3-3A inhibits the activation of TaFDL2, whereas TaFT-D1 enhances the activation of TaFDL2. The ratios of LUC to REN in *N. benthamiana* protoplasts cotransformed with reporter and effector plasmids are shown. The data from three replicates are presented as means ± SD. ** indicates a significant difference from the control at $P < 0.01$ (ANOVA).

proteins TaNaKR5 and TaFTIP7, both of which influence HD (Li et al., 2024a). However, the mechanisms underlying FT transport from leaves to grains remain to be elucidated.

The interaction modules of FT, 14-3-3 and FD are highly conserved in plants (Samach et al., 2000; Abe et al., 2005; Li and Dubcovsky, 2008; Taoka et al., 2011; Li et al., 2015; Teo et al., 2017). For example, the bZIP transcription factor FD, which is preferentially expressed in the shoot apex, is essential for FT to promote flowering in *Arabidopsis* (Abe et al., 2005). In potato, the tuber activation complex, consisting of StSP6A, StFDL1 and 14-3-3, influences tuber formation. Loss of function of *StSP6A* and *StFDL1a/b* prevents tuber formation (Teo et al., 2017). In addition, OsCEN2 affects reproductive development and negatively regulates grain size by interacting with GF14f, a 14-3-3 protein known to suppress grain growth. In the nucleus, GF14f directly binds to the transcription factor OsFD2. Overexpression of *OsFD2* reduces seed size, while knockout lines have larger seeds (He et al., 2022). In the present study, TaFT-D1 was shown to interact with 14-3-3A and TaFDL2 in wheat, acting as a coactivator of TaFDL2 in the regulation of downstream genes (Figure 6). In recent years, a series of genes related to grain weight have been cloned. However, relatively few regulatory modules for grain weight have been reported. Our study provides insight into the functions of the TaFT-D1-Ta14-3-3A-TaFDL2 module in wheat (Figure S14) and reveals a strategy for improving grain size and weight.

Diversity of *FT* and *FT-like* gene functions in plants

In *Arabidopsis*, flowering time is regulated by six major pathways: vernalization, photoperiod, ambient temperature, gibberellin, age and autonomous pathways. These pathways converge on downstream flowering genes, such as *FT* and *SOC1*, which then activate floral meristem genes to trigger flower formation (Izawa, 2021). *FT* and *FT-like* genes play crucial roles in various aspects of plant development beyond regulating flowering. In *Arabidopsis*, the *FT* gene influences lateral branch growth and axillary bud formation (Niwa et al., 2013). In rice, the Hd3a protein promotes meristematic branching (Tsuji et al., 2015). In soybeans, light-induced molecules (GmFTs and GmSTF3/4) migrate to roots to promote nodule development by stimulating gene transcription, facilitated by CCaMK activated by Rhizobium (Wang et al., 2021). In potatoes, *FT* homologues, *StSP3D* and *StSP6A*, control tuber formation (Navarro et al., 2011; Teo et al., 2017). StSP6A senses environmental cues, moves underground to induce tuber enlargement and interacts with StSWEET11 to prevent sucrose leakage (Abelenda

et al., 2019). In barley, *HvFT3* overexpression accelerates spikelet differentiation and upregulates the expression of lateral spikelet genes, thereby affecting spikelet architecture (Mulki et al., 2018). Conversely, *HvFT4* overexpression delays flowering and germination while also reducing the number of spikelets and florets, negatively impacting fertility and yield (Pieper et al., 2021). Therefore, increasing evidence indicates that *FT* and *FT-like* genes play diverse and crucial roles in plant development.

In our study, association analysis revealed that both GNS and PH were higher for the *TaFT-D1(-)* allele compared to the *TaFT-D1 (G)* allele, whereas TGW was higher for the *TaFT-D1(-)* allele (Figures 7a and S11b). Regarding the geographic distribution of breeding, *TaFT-D1(G)* is the dominant allele in the Yellow and Huai River Valley winter wheat region, as well as in the northern winter wheat region (Figure 7b). This may be related to the local farming system, where wheat varieties are required to be early maturing and high-yielding (Chen et al., 2022). In contrast, most foreign common wheat varieties carry the *TaFT-D1(-)* allele (Figure 7d). Taken together, these data suggest that the two *TaFT-D1* alleles have been widely utilized in wheat breeding to adapt the crop to specific environmental conditions. Thus, the selection and geographic distribution of *TaFT-D1* alleles play an important role in genetic improvement in wheat. Rational design of yield and quality traits is a powerful strategy to address future crop breeding challenges.

Furthermore, *FT1-Vrn3* (*qSPLN-7A.1*) is associated with increased grain number per spike (GNS), and its alleles exhibit positive additive effects on GNS (Yu et al., 2017). Three pleiotropic QTL regions are associated with SN and HD, with *TaFT-A1* being considered a candidate gene for *QTspn/HD.cau-7A* (Chen et al., 2020). The deletion of *TaFT-B1* has been found to increase the spike number under various temperature conditions, and a nonsynonymous mutation in *TaFT-B1* has been shown to significantly affect the total SN while having a minimal impact on HD (Brassac et al., 2021; Dixon et al., 2018; Finnegan et al., 2018). In this study, TaFT-D1 increased the activation of target genes related to the cell cycle and starch synthesis via TaFDL2 (Figure 6). Thus, *FT* genes are critical pleiotropic loci that regulate various traits in wheat, and their molecular regulatory network requires further exploration. Generally, early maturity and high yield have long posed a contradiction in agricultural production. Therefore, exploring flowering genes in wheat to uncouple the association between early flowering and reduced yield holds significant application value for ensuring national food security (Li et al., 2024b).
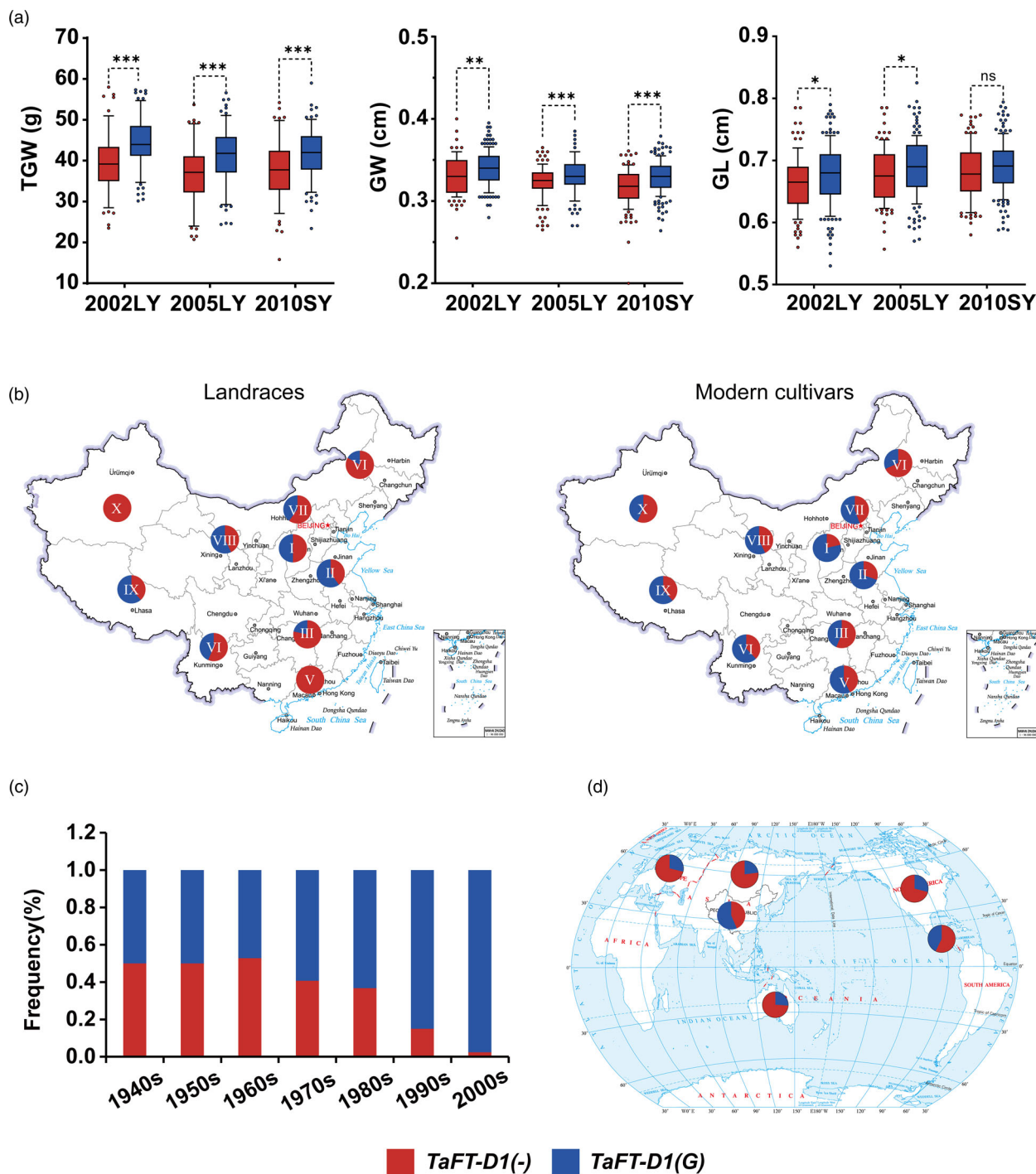
Figure 7 Association analysis, geographic distribution and frequency change in *TaFT-D1* alleles. (a) Association of *TaFT-D1* alleles with TGW, grain width (GW) and grain length (GL) in 348 modern Chinese cultivars grown in three environments. Luoyang, 2002 (2002LY); Luoyang, 2005 (2005LY); and Shunyi, 2010 (2010SY). (b) Distribution of *TaFT-D1* alleles in Chinese landraces and modern Chinese cultivars from 10 agroecological zones. I, northern winter wheat region; II, Yellow and Huai River valley winter wheat region; III, low and middle Yangtze River valley winter wheat region; IV, southwestern winter wheat region; V, southern winter wheat region; VI, northeastern spring wheat region; VII, northern spring wheat region; VIII, northwestern spring wheat region; IX, Qinghai-Tibet spring–winter wheat region; and X, Xinjiang winter–spring wheat region. (c) Changes in the frequency of *TaFT-D1* alleles during different Chinese wheat breeding periods. (d) Distribution of *TaFT-D1* alleles in major wheat regions worldwide, including China, North America, Europe, the former USSR, CIMMYT and Australia, (n = 1051). The values are presented as means ± SD. ***, ** and * indicate significant differences from the WT at $P < 0.001$, $P < 0.01$ and $P < 0.05$ (ANOVA), respectively. 'ns' indicates not significant ($P > 0.05$).

Effects of the functional divergence and dosage compensation of *TaFT-D1*, *TaFT-A1* and *TaFT-B1* on agronomic traits

Polyploid plants possess multiple genomes derived from different progenitors, resulting in increased genetic diversity. This diversity enables plants to adapt more effectively to a variety of environments and enhances their resilience against diseases and adverse climatic conditions (Cheng *et al.*, 2018). The functional differentiation of subgenomes contributes to both gene redundancy and specialization, which drive plant evolution (Chen, 2007). In agricultural breeding, this differentiation facilitates the selective introduction or enhancement of specific genes, thereby improving crop resilience, yield and quality (Zhang *et al.*, 2019). For example, the oilseed rape genome encodes four copies of the *BnaZEP* genes, which are thought to have undergone subfunctionalization; however, the potential regulatory mechanisms involved remain unclear. Genetic studies have revealed that *BnaA09.ZEP* and *BnaC09.ZEP* play specific roles in flowers, whereas *BnaA07.ZEP* and *BnaC07.ZEP* are specific to leaves (Ye *et al.*, 2024). Gene expression and interaction analyses revealed that the homologous genes of *GhCIPK6* exhibit significant functional changes in polyploids. Among these genes, *GhCIPK6D1* and *GhCIPK6D3* expression is significantly upregulated under drought stress, and functional studies have revealed that high *GhCIPK6D1* expression enhances drought sensitivity in cotton, whereas *GhCIPK6D3* expression promotes drought resistance, indicating clear functional differentiation (Sun *et al.*, 2024). Common wheat (*Triticum aestivum* L., AABBDD), an allohexaploid, contains three sets of distinct subgenomes. The diversity within its subgenomes is considered a significant factor contributing to the high plasticity of common wheat (Zhang *et al.*, 2022a). On the basis of the functional redundancy and differentiation observed among certain homologous genes within the A, B and D subgenomes of hexaploid wheat, population genetics has identified the unique allele *TaSPL6-D^{in}*, which significantly improves salt tolerance without affecting development (Wang *et al.*, 2024).

In this study, three markers for *TaFT-D1*, *TaFT-A1* and *TaFT-B1* were developed and validated in a natural population of 348 modern Chinese cultivars. *TaFT-D1* was significantly associated with TGW and GW (Figure 7a); *TaFT-A1* was associated with HD and PH (Figure S12b); and *TaFT-B1* was associated with GNS (Figure S13b). These findings suggest functional differences among the three *TaFT* homoeologous genes. However, the underlying reasons for these differences and the synergistic regulation of plant growth and development by the subgenomes remain unclear.

Dosage compensation, as a complex genetic phenomenon, may play a pivotal role in the genetic mechanisms and evolutionary processes of wheat. In our study, the knockout of *TaFT1* homoeologs demonstrated a clear dosage effect on phenotypes. Compared to the WT, TGW in *taft-1* and *taft-2* decreased by 3.5–4.7 g, HD was delayed by 1.6–1.8 days, and PH increased by 3–3.7 cm. With the knockout of *FT-B1*, *taft-4* exhibited a further decrease in TGW by 0.5–0.7 g compared to *taft-1* and *taft-2*, a 6-day delay in HD and a 2.9–3.6 cm increase in PH. Furthermore, with the knockout of *FT-A1* and *FT-B1*, TGW of *taft-5* decreased by 1.6–2.8 g, HD was delayed by 13 days, and PH increased by 4.8–5.4 cm, compared to *taft-1* and *taft-2* (Table S8). In the future, different favourable allelic or haplotype combinations of *TaFT1* homoeologs may play crucial roles in

wheat breeding by influencing key agronomic traits and enhancing the adaptability and productivity of wheat varieties. Ultimately, polyploid plants leverage the synergistic effects of their subgenomes to bolster environmental adaptability and genetic expression diversity, offering new regulatory mechanisms for plant growth and development.

Materials and methods

Plant materials and growth conditions

Chinese Spring (CS) and Kenong199 (KN199) were used in this study. For gene isolation and expression pattern analysis, various tissues of CS grown in the field at different stages were collected, while KN199 was used for gene transformation. Phenotypic traits of *taft-1* (AABBdd), *taft-2* (AABBdd), *taft-3* (AAbbDD), *taft-4* (AAbbdd) and *taft-5* (aabbdd) transgenic lines were measured in two environments: greenhouses under long-day conditions (16 h light/8 h darkness) at 23 °C and the Chinese Academy of Agricultural Sciences experimental field in Shunyi (116°65′ E, 40°13′ N), Beijing under natural conditions. And, *tafdl2* lines were also planted in the field in Shunyi (116°65′ E, 40°13′ N), Beijing. Under greenhouse conditions, transgenic and wild-type seedlings were vernalized at 4 °C for 4 weeks, then grown in the long-day conditions (16 L/8D) at 20 °C.

Additionally, 157 Chinese landraces and 348 modern Chinese cultivars, were used for genotyping and phenotyping. Among them, 476 accessions were used to perform a genome-wide association study (GWAS). Agronomic trait data for these accessions were collected from plants grown in three environments, that is, Luoyang (112°26′ E, 34°37′ N), Henan, China, in 2002 and 2005 and Shunyi (116°65′ E, 40°13′ N), Beijing, China, in 2010. Further, a total of 1051 global wheat accessions, including 384 European, 480 North American, 83 former USSR, 53 CIMMYT and 51 Australian modern cultivars, were used to investigate the global distribution of different alleles of *TaFT-D1* (Wang *et al.*, 2019).

Generation of *TaFT* CRISPR/Cas9 mutants

The different *taft* lines in the KN199 background were generated by CRISPR/Cas9-mediated genome editing. To disrupt the *TaFT* gene, a knockout construct was designed using a single guide RNA (sgRNA) that specifically targets its homoeologs. The sgRNA sequences, GAGAGCCCTCGTCCGACCATGGG, were cloned into the pBUN421 vector for CRISPR/Cas9-mediated genome editing (Zhang *et al.*, 2022b). Two independent lines with frameshift mutations of *TaFT-D1* (*taft-1* and *-2*) and lines with other types (*taft-3*, *-4* and *-5*) were screened for further analysis.

RNA-seq

The grains of WT and *taft-1* and *taft-2* lines at 15 DPA were taken for transcriptome analysis, with three biological replicates for each sample. Total RNA was isolated from the samples using TRIzol reagent (Promega, Madison, Wisconsin, USA) according to the manufacturer's instructions. The sequencing library was prepared and sequenced by Novogene (Tianjin, China) on the Illumina HiSeq platform. All clean reads were mapped to the CS reference genome V1.0 using HISAT2 software (IWGSC, 2018). The method of FPKM was used for differential expression analysis. Genes with |log2(FoldChange)| > 1 and padj <0.05 were considered as DEGs. GO function enrichment analysis and KEGG pathway enrichment analysis were performed using

clusterProfiler (Mortazavi *et al.*, 2008). The detailed information of the differentially expressed genes (DEGs) identified in a grain of *taft-d1* and WT are listed in Table S2.

Proteome analysis

WT, *taft-1* and *-2* grains at 15 DPA were analysed for protein analysis. Total protein was extracted from three biological replicates using protein extraction buffers. An appropriate amount of protein sample was taken, lysed with 50 μL lysate and digested with trypsin digestion buffer. The mixture was oscillated at 37 °C and 500 rpm for 2 h, and the enzymatic hydrolysis was terminated with a termination buffer. The peptides were desalted using the cartridges from the kit and stored at −80 °C.

The lyophilized peptides were redissolved in an A-phase (0.1% formic acid in water) solution and analysed by LC–MS/MS. The system included a timsTOF Pro2 mass spectrometer (Bruker Daltonik, Bremen, Germany) in series with the UltiMate 3000 system (Thermo Fisher Scientific, MA, USA). A total of 200 ng samples were collected. DIA data was collected using the diaPASEF mode and analysed with Spectronaut 18 software using default parameters (Lou *et al.*, 2023; Meier *et al.*, 2020). The sequence database used was Uniprot Homo_sapiens (version2023, 20 610 entries). The relevant protein information used is listed in Table S3.

RNA extraction and gene expression pattern analysis

Total RNA was extracted from different wheat tissues using RNAiso Plus reagent (Takara Bio, China), and cDNA was synthesized using the FastKing RT Kit (Tiangen, Beijing). TB® Green Premix Ex Taq™ (TaKaRa, Japan) was used on the Roche LightCycler® 96 thermal cycler (Roche Applied Science, Mannheim, Germany). Actin was used as the internal reference (Li *et al.*, 2023). Each measurement was performed independently three times. Quantitative changes were assessed using the $2^{-\Delta\Delta CT}$ method (Livak and Schmittgen, 2001). The detailed information of the primers used in this study is listed in Table S9.

Subcellular localization and transcriptional activity analysis

For the subcellular localization of *TaFT*, the full-length encoding sequence (CDS) of *TaFT-D1(G)* and the pre-terminated sequence of *TaFT-D1(−)* were amplified from CS cDNA and cloned into the pJIT163-GFP vector. The recombinant vector and control vector (pJIT163-GFP) were transformed into wheat protoplasts by the PEG-mediated method (Zheng *et al.*, 2014). After incubation at 22°C in continuous darkness for 16 h, the fluorescence of GFP was observed under a LSM880 confocal microscope (Zeiss, Oberkochen, Germany) at 550 nm.

To determine the transcriptional activity of *TaFDL2*, a dual-luciferase reporter assay was conducted in tobacco (*N. benthamiana*) using 5 × GAL4-LUC-NOS, 35S-REN-NOS and 35S-GAL4DB-NOS vectors as reporter and effector constructs (Li *et al.*, 2016). *TaFDL2* was cloned into the 35S-GAL4DB-NOS vector, and then the TaFDL2-GAL4DB, 5 × GAL4-LUC-NOS, and 35S-REN-NOS vectors were co-transfected into tobacco (*N. benthamiana*). The luciferase activity of Herpes Simplex Virus 16 (VP16) was determined, with 35S-GAL4-DB as the negative control and Herpes Simplex Virus 16 as the positive control (Wei *et al.*, 2015).

LCI assays and BiFC assays

The interaction between TaFT-D1, TaFDL2 and Ta14-3-3A was analysed in the leaves of tobacco (*N. benthamiana*). Full-length *TaFT-D1*, *TaFDL2* and *Ta14-3-3A* CDS were fused to the N-terminal and C-terminal regions of the luciferase reporter gene LUC, respectively, and then transformed into GV3101 cells. The cells carrying the recombinant vectors of nLUC and cLUC were transfected into tobacco leaves. After 48 h of culture, LUC activity was imaged and analysed using the NightSHADE LB 985 plant imaging system (Berthold Technologies, Bad Wildbad, Germany). In the BiFC assays, GV3101 cells containing the recombinant vectors of TaFT-D1-nYFP, Ta14-3-3A-cYFP and TaFDL2-nYFP were transfected into tobacco leaves. After 48–72 h, the fluorescence signal of YFP was observed under the LSM880 confocal laser scanning microscope (Zeiss, Oberkochen, Germany).

Dual-LUC reporter system assay

Based on previous studies, the instantaneous determination of transcriptional activity in tobacco (*N. benthamiana*) was performed using the DLR assay (Hellens *et al.*, 2005). The 2-kb promoter sequences of downstream genes and CDS of *TaFT-D1*, *TaFDL2* and *Ta14-3-3A* were cloned into pGreenII 0800-LUC and pGreenII 62-SK, respectively, to obtain the reporters and effectors. With the help of the pSoup-p19 vector, the reporters and effectors were transformed into GV3101 cells and then co-transfected into tobacco leaves. After incubation for 60 h, LUC and REN activity were measured using the DLR assay system (Yeasen, Shanghai, China).

Yeast experiments

The relationship between TaFDL2 and *TaNAC19-3A/TaSWEET15-like-7B/TaCYC3;2/TaCYC4;1* was analysed by Y1H. Full-length CDS containing *TaFDL2* were cloned into pB42AD vectors, and promoters containing possible binding motifs were cloned into pLacZi vectors as reporter vectors. TaFDL2-pB42AD and reporter vectors were transformed into yeast strains EGY48. The co-transformed yeast strains were cultured on SD/-Trp/-Ura medium at 30 °C for about 2 days. Then, droplets of the positive colonies were added to the SD/-Trp/-Ura/X-gal medium. After incubation for 1–2 days under the same conditions, the colonies were observed for blue coloration in the Y2H experiment, CDS of *TaFT-D1*, *Ta14-3-3A* and *TaFDL2* were independently cloned into pGADT7 and pGBKT7 vectors, respectively. The TaFT-D1/TaFDL2/Ta14-3-3A-BD and TaFDL2/Ta14-3-3A-AD vectors were generated. The above vectors were transformed into the Y2H Gold yeast strains. The interaction was determined by the growth of co-transformed yeast strains on SD/-Trp/-Leu medium and then on SD/-Trp/-Leu/-His/-Ade.

Microscopy and cell size measurement and scanning electron microscopy

The grains of WT and *taft-1* and *taft-2* lines were fixed with formalin-5% acetic acid-70% alcohol (FAA) solution for 15 DPA. The samples were dehydrated in a series of ethanol solutions (75%, 85%, 90%, 95% and 100%; v/v), permeated with xylene and embedded in paraffin. Tissue sections (4 μm) were cut on a microtome (Leica Microsystems, Nussloch, Germany) and stained with toluidine blue. The slices were imaged under the SteREO Discovery V20 microscope (Carl Zeiss).

The grains of WT and *taft-1* and *taft-2* strains at 20 DPA were transversely cut into 1 mm slices and coated with gold powder. The samples were observed using a Hitachi S-3400N (Hitachi, Tokyo, Japan) scanning electron microscope.

The wheat grains were ground into flour, and the total starch content was determined using the starch determination kit (Megazyme, Wicklow, Ireland) according to the manufacturer's method. The amylopectin content was determined according to the Chinese national standard method (GB/T 15683-2008).

Electrophoretic mobility shift assay

The full-length *TaFDL2* CDS was amplified and cloned into the pET-28a(+) (Merck Millipore, Burlington, MA, USA) vector. Protein expression and purification were performed according to previous protocols (Jian *et al.*, 2024). TaFDL2-His was purified using Ni-NTA resin (Qiagen, Germany). The 5′-biotin labelled probe (100 fmol) and unlabeled common primer (WT) were used as competitors, and a mutated common primer (mu) was used with 1 μg HIS-TaFDL2 protein, 1 × binding buffer, 2.5% glycerol, 5 mmol/L MgCl$_2$ and 1 μL poly (dI-dC). The mixture was incubated at room temperature for 30 min. Subsequently, protein-DNA complexes were isolated by 0.5 × Tris-borate-EDTA (TBE), 6% polyacrylamide gel electrophoresis and transferred to a Hybond-N+ nylon membrane (Amersham, USA). The Light Shift chemiluminescence EMSA kit (Thermo Scientific, USA) was used according to the manufacturer's instructions.

GWAS

The Affymetrix Axiom Wheat660 array containing 630 517 SNPs (Sun *et al.*, 2020) was used for genotyping materials, yielding 350 497 polymorphic SNPs after filtering (DQC >0.6, QC call rate >70%, MAF ≥0.05, missing rate ≤0.2) (Jiao *et al.*, 2023). Using the mixed linear model (MLM) of the EMMAX software package, phenotypic data of thousand-grain weight (g), plant height (cm) and heading date (day), along with 350 497 polymorphic SNPs from a Wheat660K SNP array, were used to perform genome-wide association study in a natural population composed of 476 accessions (Kang *et al.*, 2010; Wang *et al.*, 2021). The significance threshold for the whole genome was set to $P \leq 10^{-4}$. A Q matrix was constructed using the first three principal components, and population structure correction was performed using GCTA software (Yang *et al.*, 2011). Genetic relationships between individuals were modelled using EMMAX's kinship matrix as a random effect (Kang *et al.*, 2010).

KASP and dCAPS marker development and validation

Based on re-sequencing data (http://wheat.cau.edu.cn/WheatUnion) mining and detecting sequence polymorphisms of *TaFT-D1*, KASP markers were developed for high-throughput genotyping in 157 Chinese landraces, 348 modern Chinese cultivars and 1051 introduced wheat varieties (Hao *et al.*, 2020). The fluorescence signal was detected by QuantStudioTM 7 Flex (ABI, USA), and the data were displayed using QuantStudioTM Real-time PCR software v.1.3 (ABI, USA). According to the polymorphisms of *TaFT-A1* and *TaFT-B1*, dCAPS markers, incubating with the restriction enzyme *Fok* I and distinguishing by 4% agarose gel, were developed and utilized to genotype all materials above-mentioned. The genotyping data of all materials used in this study are listed in Tables S4 and S5. Significance of difference analysis for the alleles of *TaFT-A1, -B1, -D1* was performed as described earlier (Wang *et al.*, 2019). To further validate the genetic effect and phenotypic variance explained

(PVE) of markers for three homologous genes, the genetic effect value is calculated according to the difference of the phenotypic means between alleles. The phenotypic variance explained (PVE) is the ratio of the total variance of the SNP effects to the total phenotypic variance, represented as PVE = Var(bX)/Var(Y) (Tang *et al.*, 2022).

Statistical analysis

DNA sequence alignments were performed using DNAMAN (9.0, Lynnon, Quebec, Canada). Descriptive statistics, one-way ANOVA and Tukey/LSD tests were performed using SPSS (IBM, Armonk, NY, USA) for variance and significance analysis. Graphs were drawn using GraphPad Prism (8.0, San Diego, USA), and Figures were combined using Adobe Illustrator (24.0, Adobe, USA).

Author contributions

Chenyang Hao, Tian Li and Jian Hou planned and designed the research. Yinhui Zhang performed experiments, performed phenotypic evaluation and wrote the manuscript. Xuemei Si participated in manuscript writing and arranged pictures. All authors collected the data, and Haixia Liu performed GWAS. Chenyang Hao, Tian Li and Jian Hou provided advice about the experiments and revised the manuscript. All authors have read and approved the manuscript.

Acknowledgements

Conflicts of interest

The authors declare no conflict of interest.

Data availability statement

The data that support the findings of this study are available on request from the corresponding author. The data are not publicly available due to privacy or ethical restrictions.

References

Abe, M., Kobayashi, Y., Yamamoto, S., Daimon, Y., Yamaguchi, A., Ikeda, Y., Ichinoki, H. *et al.* (2005) FD, a bZIP protein mediating signals from the floral pathway integrator FT at the shoot apex. *Science* **309**, 1052–1056.

Abelenda, J.A., Bergonzi, S., Oortwijn, M., Sonnewald, S., Du, M., Visser, R.G.F., Sonnewald, U. *et al.* (2019) Source-sink regulation is mediated by interaction of an FT homolog with a SWEET protein in potato. *Curr. Biol.* **29**, 1178–1186.

Brassac, J., Muqaddasi, Q.H., Plieske, J., Ganal, M.W. and Röder, M.S. (2021) Linkage mapping identifies a non-synonymous mutation in *FLOWERING LOCUS T* (*FT-B1*) increasing spikelet number per spike. *Sci. Rep.* **11**, 1585.

Chen, Z.J. (2007) Genetic and epigenetic mechanisms for gene expression and phenotypic variation in plant polyploids. *Annu. Rev. Plant Biol.* **58**, 377–406.

Chen, Z.Y., Cheng, X.J., Chai, L.L., Wang, Z.H., Du, D.J., Wang, Z.H., Bian, R.L. *et al.* (2020) Pleiotropic QTL influencing spikelet number and heading date in common wheat (*Triticum aestivum* L.). *Theor. Appl. Genet.* **133**, 1825–1838.

Chen, Z.Y., Ke, W.S., He, F., Chai, L.L., Cheng, X.J., Xu, H.W., Wang, X.B. *et al.* (2022) A single nucleotide deletion in the third exon of *FT-D1* increases the spikelet number and delays heading date in wheat (*Triticum aestivum* L.). *Plant Biotechnol. J.* **20**, 920–933.

Cheng, F., Wu, J., Cai, X., Liang, J.L., Freeling, M. and Wang, X.W. (2018) Gene retention, fractionation and subgenome differences in polyploid plants. *Nat. Plants* **4**, 258–268.

Dixon, L.E., Farré, A., Finnegan, E.J., Orford, S., Griffiths, S. and Boden, S.A. (2018) Developmental responses of bread wheat to changes in ambient temperature following deletion of a locus that includes *FLOWERING LOCUS T*. *Plant Cell Environ.* **41**, 1715–1725.

Finnegan, E.J., Ford, B., Wallace, X.M., Pettolino, F., Griffin, P.T., Schmitz, R.J., Zhang, P. *et al.* (2018) Zebularine treatment is associated with deletion of *FT-B1* leading to an increase in spikelet number in bread wheat. *Plant Cell Environ.* **41**, 1346–1360.

Gao, Y.J., An, K.X., Guo, W.W., Chen, Y.M., Zhang, R.J., Zhang, X., Chang, S.Y. *et al.* (2021) The endosperm-specific transcription factor *TaNAC019* regulates glutenin and starch accumulation and its elite allele improves wheat grain quality. *Plant Cell* **33**, 603–622.

Gao, Y.J., Li, Y.S., Xia, W.Y., Dai, M.Q., Dai, Y., Wang, Y.G., Ma, H.G. *et al.* (2023) The regulation of grain weight in wheat. *Seed Biology* **2**, 17.

Hao, C.Y., Jiao, C.Z., Hou, J., Li, T., Liu, H.X., Wang, Y.Q., Zheng, J. *et al.* (2020) Resequencing of 145 landmark cultivars reveals asymmetric sub-genome selection and strong founder genotype effects on wheat breeding in China. *Mol. Plant* **13**, 1733–1751.

He, Y., Li, L.Y., Shi, W.B., Tan, J.H., Luo, X.X., Zheng, S.Y., Chen, W.T. *et al.* (2022) Florigen repression complexes involving rice CENTRORADIALIS2 regulate grain size. *Plant Physiol.* **190**, 1260–1274.

Hellens, R.P., Allan, A.C., Friel, E.N., Bolitho, K., Grafton, K., Templeton, M.D., Karunairetnam, S. *et al.* (2005) Transient expression vectors for functional genomics, quantification of promoter activity and RNA silencing in plants. *Plant Methods* **1**, 13.

Hou, J., Jiang, Q.Y., Hao, C.Y., Wang, Y.Q., Zhang, H.N. and Zhang, X.Y. (2014) Global selection on sucrose synthase haplotypes during a century of wheat breeding. *Plant Physiol.* **164**, 1918–1929.

IWGSC. (2018) Shifting the limits in wheat research and breeding using a fully annotated reference genome. *Science* **361**, eaar7191.

Izawa, T. (2021) What is going on with the hormonal control of flowering in plants? *Plant J.* **105**, 431–445.

Jia, M.L., Li, Y.N., Wang, Z.Y., Tao, S., Sun, G.L., Kong, X.C., Wang, K. *et al.* (2021) TaIAA21 represses TaARF25-mediated expression of *TaERFs* required for grain size and weight development in wheat. *Plant J.* **108**, 1754–1767.

Jian, C., Pan, Y.X., Liu, S.J., Guo, M.J., Huang, Y.L., Cao, L.N., Zhang, W.J. *et al.* (2024) The TaGW2-TaSPL14 module regulates the trade-off between tiller number and grain weight in wheat. *J. Integr. Plant Biol.* **66**, 1953–1965.

Jiang, Q.Y., Hou, J., Hao, C.Y., Wang, L.F., Ge, H.M., Dong, Y.S. and Zhang, X.Y. (2011) The wheat (*T. aestivum*) sucrose synthase 2 gene (*TaSus2*) active in endosperm development is associated with yield traits. *Funct. Integr. Genomics* **11**, 49–61.

Jiao, C.Z., Hao, C.Y., Li, T., Bohra, A., Wang, L.F., Hou, J., Liu, H.X. *et al.* (2023) Fast integration and accumulation of beneficial breeding alleles through an AB–NAMIC strategy in wheat. *Plant Commun.* **4**, 100549.

Jin, S.Y., Nasim, Z., Susila, H. and Ahn, J.H. (2021) Evolution and functional diversification of *FLOWERING LOCUS T/TERMINAL FLOWER 1* family genes in plants. *Semin. Cell Dev. Biol.* **109**, 20–30.

Kang, H.M., Sul, J.H., Service, S.K., Zaitlen, N.A., Kong, S.Y., Freimer, N.B., Sabatti, C. *et al.* (2010) Variance component model to account for sample structure in genome-wide association studies. *Nat. Genet.* **42**, 348–354.

Kardailsky, I., Shukla, V.K., Ahn, J.H., Dagenais, N., Christensen, S.K., Nguyen, J.T., Chory, J. *et al.* (1999) Activation tagging of the floral inducer *FT*. *Science* **286**, 1962–1965.

Kobayashi, Y., Kaya, H., Goto, K., Iwabuchi, M. and Araki, T. (1999) A pair of related genes with antagonistic roles in mediating flowering signals. *Science* **286**, 1960–1962.

Li, C.X. and Dubcovsky, J. (2008) Wheat FT protein regulates *VRN1* transcription through interactions with FDL2. *Plant J.* **55**, 543–554.

Li, C.X., Lin, H.Q. and Dubcovsky, J. (2015) Factorial combinations of protein interactions generate a multiplicity of florigen activation complexes in wheat and barley. *Plant J.* **84**, 70–82.

Li, T., Wu, X.Y., Li, H., Song, J.H. and Liu, J.Y. (2016) A dual-function transcription factor, AtYY1, is a novel negative regulator of the *Arabidopsis* ABA response network. *Mol. Plant* **9**, 650–661.

Li, H.F., Liu, H., Hao, C.Y., Li, T., Liu, Y.C., Wang, X.L., Yang, Y.X. *et al.* (2023) The auxin response factor TaARF15-A1 negatively regulates senescence in common wheat (*Triticum aestivum* L.). *Plant Physiol.* **191**, 1254–1271.

Li, Y.T., Xiong, H.C., Guo, H.J., Xie, Y.D., Zhao, L.S., Gu, J.Y., Li, H.Y. *et al.* (2024a) A gain-of-function mutation at the C-terminus of FT-D1 promotes heading by interacting with 14-3-3A and FDL6 in wheat. *Plant Biotechnol. J.* **23**, 20–35.

Li, Y.F., Zhang, L.Y., Wang, J., Wang, X., Guo, S.Y., Xu, Z.J., Li, D.L. *et al.* (2024b) Flowering time regulator *qFT13-3* involved in soybean adaptation to high latitudes. *Plant Biotechnol. J.* **22**, 1164–1176.

Liu, L., Li, C.Y., Teo, Z.W.N., Zhang, B. and Yu, H. (2019) The MCTP-SNARE complex regulates florigen transport in *Arabidopsis*. *Plant Cell* **31**, 2475–2490.

Liu, L., Zhang, Y. and Yu, H. (2020a) Florigen trafficking integrates photoperiod and temperature signals in *Arabidopsis*. *J. Integr. Plant Biol.* **62**, 1385–1398.

Liu, H., Li, H.F., Hao, C.Y., Wang, K., Wang, Y.M., Qin, L., An, D.G. *et al.* (2020b) TaDA1, a conserved negative regulator of kernel size, has an additive effect with *TaGW2* in common wheat (*Triticum aestivum* L.). *Plant Biotechnol. J.* **18**, 1330–1342.

Liu, H.X., Si, X.M., Wang, Z.Y., Cao, L.J., Gao, L.F., Zhou, X.L., Wang, W.X. *et al.* (2023) TaTPP-7A positively feedback regulates grain filling and wheat grain yield through T6P-SnRK1 signalling pathway and sugar-ABA interaction. *Plant Biotechnol. J.* **21**, 1159–1175.

Livak, K.J. and Schmittgen, T.D. (2001) Analysis of relative gene expression data using real-time quantitative PCR and the 2(-Delta Delta C(T)) Method. *Methods* **25**, 402–408.

Lou, R.H., Cao, Y., Li, S.S., Lang, X.Y., Li, Y.X., Zhang, Y.Y. and Shui, W.Q. (2023) Benchmarking commonly used software suites and analysis workflows for DIA proteomics and phosphoproteomics. *Nat. Commun.* **14**, 94.

Lyu, J.Y., Wang, D.Z., Sun, N., Yang, F., Li, X.P., Mu, J.Y., Zhou, R.X. *et al.* (2024) The TaSnRK1-TabHLH489 module integrates brassinosteroid and sugar signalling to regulate the grain length in bread wheat. *Plant Biotechnol. J.* **22**, 1989–2006.

Meier, F., Brunner, A.D., Frank, M., Ha, A., Bludau, I., Voytik, E., Kaspar-Schoenefeld, S. *et al.* (2020) diaPASEF: parallel accumulation-serial fragmentation combined with data-independent acquisition. *Nat. Methods* **17**, 1229–1236.

Mortazavi, A., Williams, B.A., McCue, K., Schaeffer, L. and Wold, B. (2008) Mapping and quantifying mammalian transcriptomes by RNA-Seq. *Nat. Methods* **5**, 621–628.

Mulki, M.A., Bi, X. and Korff, M.V. (2018) *FLOWERING LOCUS T3* controls spikelet initiation but not floral development. *Plant Physiol.* **178**, 1170–1186.

Navarro, C., Abelenda, J.A., Cruz-Oró, E., Cuéllar, C.A., Tamaki, S., Silva, J., Shimamoto, K. *et al.* (2011) Control of flowering and storage organ formation in potato by *FLOWERING LOCUS T*. *Nature* **478**, 119–122.

Niwa, M., Endo, M. and Araki, T. (2013) Florigen is involved in axillary bud development at multiple stages in *Arabidopsis*. *Plant Signal. Behav.* **8**, e27167.

Pieper, R., Tomé, F., Pankin, A. and Korff, M.V. (2021) *FLOWERING LOCUS T4* delays flowering and decreases floret fertility in barley. *J. Exp. Bot.* **72**, 107–121.

Samach, A., Onouchi, H., Gold, S.E., Ditta, G.S., Schwarz-Sommer, Z., Yanofsky, M.F. and Coupland, G. (2000) Distinct roles of CONSTANS target genes in reproductive development of *Arabidopsis*. *Science* **288**, 1613–1616.

Shen, J., Zhang, L., Wang, H.Y., Guo, J.Z., Li, Y.C., Tan, Y.Y., Shu, Q.Y. *et al.* (2024) The phosphatidylethanolamine-binding proteins OsMFT1 and OsMFT2 regulate seed dormancy in rice. *Plant Cell* **36**, 3857–3874.

Su, Z.Q., Hao, C.Y., Wang, L.F., Dong, Y.C. and Zhang, X.Y. (2011) Identification and development of a functional marker of TaGW2 associated with grain weight in bread wheat (*Triticum aestivum* L.). *Theor. Appl. Genet.* **122**, 211–223.

Sun, C.W., Dong, Z.D., Zhao, L., Ren, Y., Zhang, N. and Chen, F. (2020) The Wheat 660K SNP array demonstrates great potential for marker-assisted selection in polyploid wheat. *Plant Biotechnol. J.* **18**, 1354–1360.

Sun, W.N., Xia, L.J., Deng, J.W., Sun, S.M., Yue, D.D., You, J.Q., Wang, M.J. et al. (2024) Evolution and subfunctionalization of CIPK6 homologous genes in regulating cotton drought resistance. Nat. Commun. **15**, 5733.

Tamaki, S., Matsuo, S., Wong, H.L., Yokoi, S. and Shimamoto, K. (2007) Hd3a protein is a mobile flowering signal in rice. Science **316**, 1033–1036.

Tang, M.S., Wang, T. and Zhang, X.F. (2022) A review of SNP heritability estimation methods. Brief. Bioinform. **23**, bbac067.

Taoka, K.I., Ohki, I., Tsuji, H., Furuita, K., Hayashi, K., Yanase, T., Yamaguchi, M. et al. (2011) 14-3-3 proteins act as intracellular receptors for rice Hd3a florigen. Nature **476**, 332–335.

Teo, C.J., Takahashi, K., Shimizu, K., Shimamoto, K. and Taoka, K.I. (2017) Potato tuber induction is regulated by interactions between components of a tuberigen complex. Plant Cell Physiol. **58**, 365–374.

Tsuji, H., Tachibana, C., Tamaki, S., Taoka, K.I., Kyozuka, J. and Shimamoto, K. (2015) Hd3a promotes lateral branching in rice. Plant J. **82**, 256–266.

Wang, Y.M., Hou, J., Liu, H., Li, T., Wang, K., Hao, C.Y., Liu, X. et al. (2019) TaBT1, affecting starch synthesis and thousand kernel weight, underwent strong selection during wheat improvement. J. Exp. Bot. **70**, 1497–1511.

Wang, Z.W., Hao, C.Y., Zhao, J., Li, C., Jiao, C.Z., Xi, W., Hou, J. et al. (2021) Genomic footprints of wheat evolution in China reflected by a Wheat660K SNP array. Crop J. **9**, 29–41.

Wang, T., Guo, J., Peng, Y.Q., Lyu, X.G., Liu, B., Sun, S.Y. and Wang, X.L. (2021) Light-induced mobile factors from shoots regulate rhizobium-triggered soybean root nodulation. Science **374**, 65–71.

Wang, J.J., Zhang, C., Chen, Y.P., Shao, Y.N., Liao, M.F., Hou, Q., Zhang, W.T. et al. (2023) The BnTFL1-BnGF14nu-BnFD module regulates flower development and plant architecture in Brassica napus. Crop J. **11**, 1696–1710.

Wang, M., Cheng, J., Wu, J.H., Chen, J.F., Liu, D., Wang, C.Y., Ma, S.W. et al. (2024) Variation in TaSPL6-D confers salinity tolerance in bread wheat by activating TaHKT1;5-D while preserving yield-related traits. Nat. Genet. **56**, 1257–1269.

Wei, W., Zhang, Y.Q., Tao, J.J., Chen, H.W., Li, Q.T., Zhang, W.K., Ma, B. et al. (2015) The Alfin-like homeodomain finger protein AL5 suppresses multiple negative factors to confer abiotic stress tolerance in Arabidopsis. Plant J. **81**, 871–883.

Yang, J., Lee, S.H., Goddard, M.E. and Visscher, P.M. (2011) GCTA: a tool for genome-wide complex trait analysis. Am. J. Hum. Genet. **88**, 76–82.

Ye, S.H., Huang, Y.Y., Ma, T.T., Ma, X.W., Li, R.H., Shen, J.X. and Wen, J. (2024) BnaABF3 and BnaMYB44 regulate the transcription of zeaxanthin epoxidase genes in carotenoid and abscisic acid biosynthesis. Plant Physiol. **195**, 2372–2388.

Yu, K., Liu, D.C., Wu, W.Y., Yang, W.L., Sun, J.Z., Li, X., Zhan, K.H. et al. (2017) Development of an integrated linkage map of einkorn wheat and its application for QTL mapping and genome sequence anchoring. Theor. Appl. Genet. **130**, 53–70.

Zhai, H., Wan, Z., Jiao, S., Zhou, J.W., Xu, K., Nan, H.Y., Liu, Y.X. et al. (2022) GmMDE genes bridge the maturity gene E1 and florigens in photoperiodic regulation of flowering in soybean. Plant Physiol. **189**, 1021–1036.

Zhang, L., Zhao, Y.L., Gao, L.F., Zhao, G.Y., Zhou, R.H., Zhang, B.S. and Jia, J.Z. (2012) TaCKX6-D1, the ortholog of rice OsCKX2, is associated with grain weight in hexaploid wheat. New Phytol. **195**, 574–584.

Zhang, K., Wang, X.W. and Cheng, F. (2019) Plant polyploidy: origin, evolution, and its influence on crop domestication. Hort. Plant J. **5**, 231–239.

Zhang, B., Li, C.X., Li, Y. and Yu, H. (2020) Mobile TERMINAL FLOWER1 determines seed size in Arabidopsis. Nature Plants **6**, 1146–1157.

Zhang, Y.Y., Li, Z.J., Liu, J.Y., Zhang, Y.E., Ye, L.H., Peng, Y., Wang, H.Y. et al. (2022a) Transposable elements orchestrate subgenome-convergent and -divergent transcription in common wheat. Nat. Commun. **13**, 6940.

Zhang, X.Y., Jia, H.Y., Li, T., Wu, J.Z., Nagarajan, R., Lei, L., Powers, C. et al. (2022b) TaCol-B5 modifies spike architecture and enhances grain yield in wheat. Science **376**, 180–183.

Zhang, J.N., Zhang, Z.H., Zhang, R.J., Yang, C.F., Zhang, X.B., Chang, S.Y., Chen, Q. et al. (2024) Type I MADS-box transcription factor TaMADS-GS regulates grain size by stabilizing cytokinin signalling during endosperm cellularization in wheat. Plant Biotechnol. J. **22**, 200–215.

Zheng, J., Liu, H., Wang, Y.Q., Wang, L.F., Chang, X.P., Jing, R.L., Hao, C.Y. et al. (2014) TEF-7A, a transcript elongation factor gene, influences yield-related traits in bread wheat (Triticum aestivum L.). J. Exp. Bot. **65**, 5351–5365.

Zhu, Y., Liu, L., Shen, L.S. and Yu, H. (2016) NaKR1 regulates long-distance movement of FLOWERING LOCUS T in Arabidopsis. Nature Plants. **2**, 16075.

Zicola, J., Liu, L.Y., Tänzler, P. and Turck, F. (2019) Targeted DNA methylation represses two enhancers of FLOWERING LOCUS T in Arabidopsis thaliana. Nature Plants **5**, 300–307.

Supporting information

Additional supporting information may be found online in the Supporting Information section at the end of the article.

Figure S1 FT-D1 was identified as a candidate gene controlling heading date (HD) and plant height (PH) on chromosome 7D through GWAS.

Figure S2 Gene structure of TraesCS7D02G111500 and its association analysis with TGW, PH and HD.

Figure S3 Characterization of TaFT in wheat.

Figure S4 Target site for TaFT and phenotypic differences on other agronomic traits between the WT and taft lines.

Figure S5 Comparison of phenotypes of WT and taft lines grown in greenhouses.

Figure S6 GO classification of DEGs based on RNA-seq analysis and RT-qPCR analysis of other down-regulated genes in grains of WT and taft-d1 lines at 15 DPA.

Figure S7 Expression map of TaFD-like in different tissues.

Figure S8 Functional characterization of TaFDL2 in wheat.

Figure S9 Expression map of Ta14-3-3 in different tissues.

Figure S10 TaFT-D1(-) does not promote the activation of FDL2.

Figure S11 TaFT-D1 alleles-based KASP marker development and their association with other agronomic traits in modern Chinese cultivars.

Figure S12 Marker development, association analysis and geographic distribution of TaFT-A1 alleles.

Figure S13 Marker development, association analysis and geographic distribution of TaFT-B1 alleles.

Figure S14 A proposed working model of how FT-D1 regulates grain weight in common wheat.

Table S1 Thirteen high-confidence genes predicted in the 2 Mb interval (68 720 858–70 720 858 Mb) on chromosome 7D.

Table S2 Differentially expressed genes (DEGs) identified in a grain of taft-d1 and WT.

Table S3 Differently abundant proteins in a grain of taft-d1 and WT.

Table S4 Detailed information and genotypes of 157 Chinese wheat landraces and 348 modern Chinese cultivars.

Table S5 Detailed information and genotypes of 1051 global accessions.

Table S6 Genetic effect values of markers for TaFT-A1, TaFT-B1 and TaFT-D1 in 348 modern Chinese cultivars.

Table S7 Phenotypic variance explained of markers for TaFT-A1, TaFT-B1 and TaFT-D1 in 348 modern Chinese cultivars.

Table S8 Multiple comparisons of TGW, PH and HD between different lines.

Table S9 Primers used in this study.